UCID - 16639

LAWRENCE LIVERMORE LABORATORY

University of California/Livermore, California

COAL FRACTURE MEASUREMENTS USING IN SITU ELECTRICAL METHODS: PRELIMINARY RESULTS

R. J. Lytle

E. F. Laine

D. L. Lager

November 20, 1974

Prepared for U. S. Atomic Energy Commission under contract no. W-7405-Eng-48

DISCLAIMER

CONTENTS

COAL FRACTURE MEASUREMENTS USING IN SITU METHODS: PRELIMINARY RESULTS

ABSTRACT

Subsurface electrical profiles have been measured and evaluated for the coal fracturization site at Kemmerer, Wyoming. Both high-frequency (1- to 51-MHz) and low-frequency (20-Hz) data yielded consistent subsurface profiles. Measurements were made on the surface, in a single drill hole, and between drill holes separated by 9 m (30 ft). The results show that field interpretation of data is feasible and can be done routinely, also that both high-frequency and low-frequency techniques give good resolution. Techniques are described for determining three-dimensional permeability in situ via electrical methods. Sophisticated data inversion algorithms have been developed that yield accurate subsurface models from real (noisy) data. An overview is given of the experimental methods, the data, and the procedures for data interpretation. Electrical methods show much promise as a monitoring tool for coal-field experiments.

INTRODUCTION

This Laboratory is performing a series of experiments in underground coal fracturing near Kemmerer, Wyoming (Fig. 1), on land made available to it by the Kemmerer Coal Company. The site of the experiments is a strip mine located at the top of a ridge at about 2600 m (7500 ft) altitude. The coal outcrops reveal seams of various thicknesses that meet the surface at an angle of 18 deg (Fig. 2). The area is strip-mined to expose the ends of the coal seams, which vary in thickness from 1.5 m (5 ft) to about 27 m (90 ft) for the main seam. The overburden consists of sedimentary clay-layered deposits. The main coal seam is at the bottom of a pit and is exposed over its full horizontal width.

The purpose of these experiments is to characterize the physical properties of the coal before and after fracturing induced by high explosives detonated in the coal bed. The information will contribute significantly to the establishment of the best techniques for future large-scale underground coal-conversion projects (e.g., in situ coal gasification).

Electrical methods can be used to monitor the subsurface conditions before and after the high explosive detonation. It is hoped that these electrical methods will permit comparisons of preshot and postshot subsurface electrical profiles to determine the volume of coal fractured by the detonation. Here we report the preliminary analyses of the preshot subsurface conditions as revealed by electical probing procedures. Both high-frequency (HF) and low-frequency (LF) electrical procedures were applied successfully using equipment and expertise that are readily available at LLL.

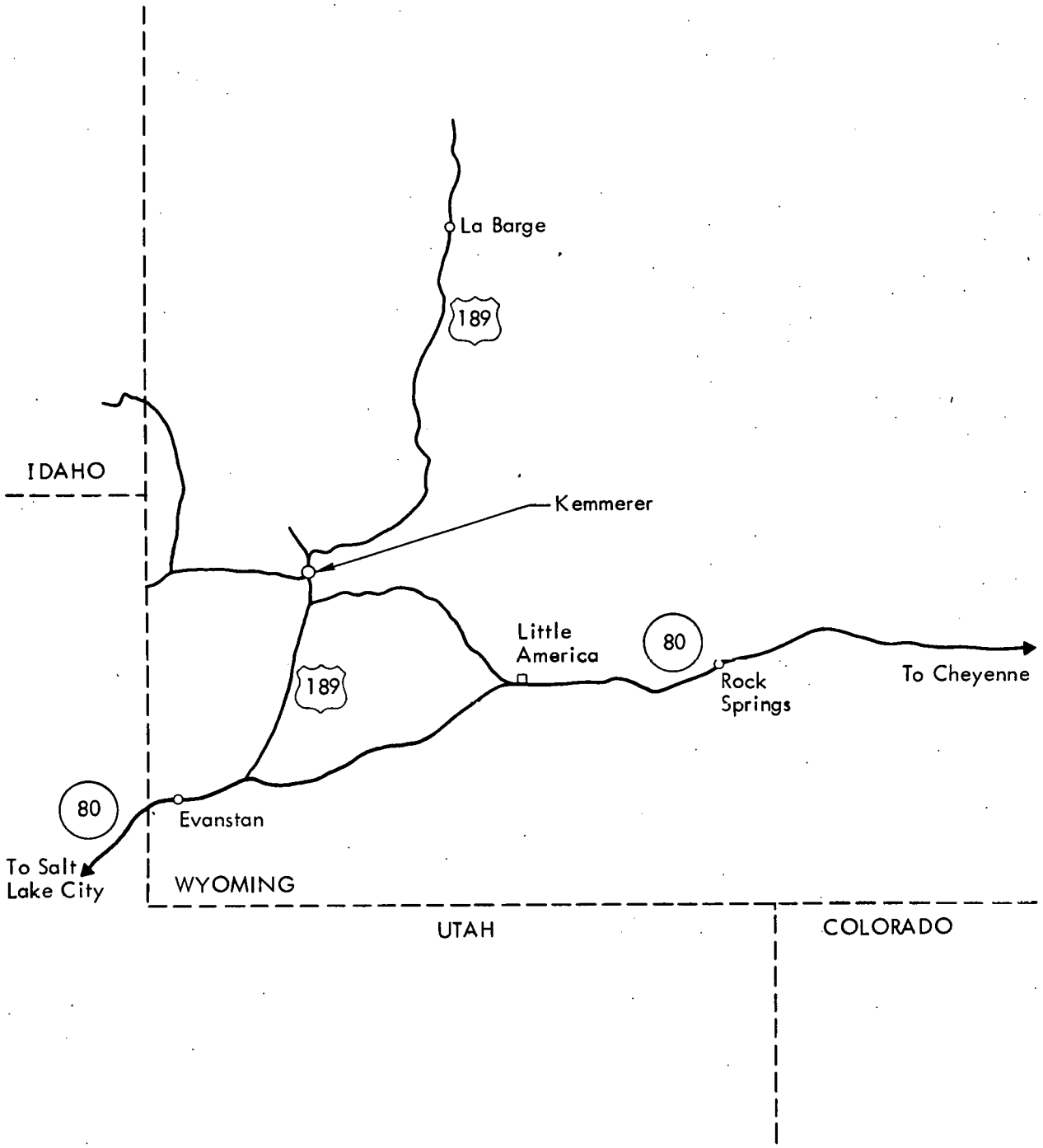

Fig. 1. The Kemmerer site is in the southwest corner of Wyoming. Personnel travel to the site from Salt Lake City (about 2-1/2 hr surface travel time).

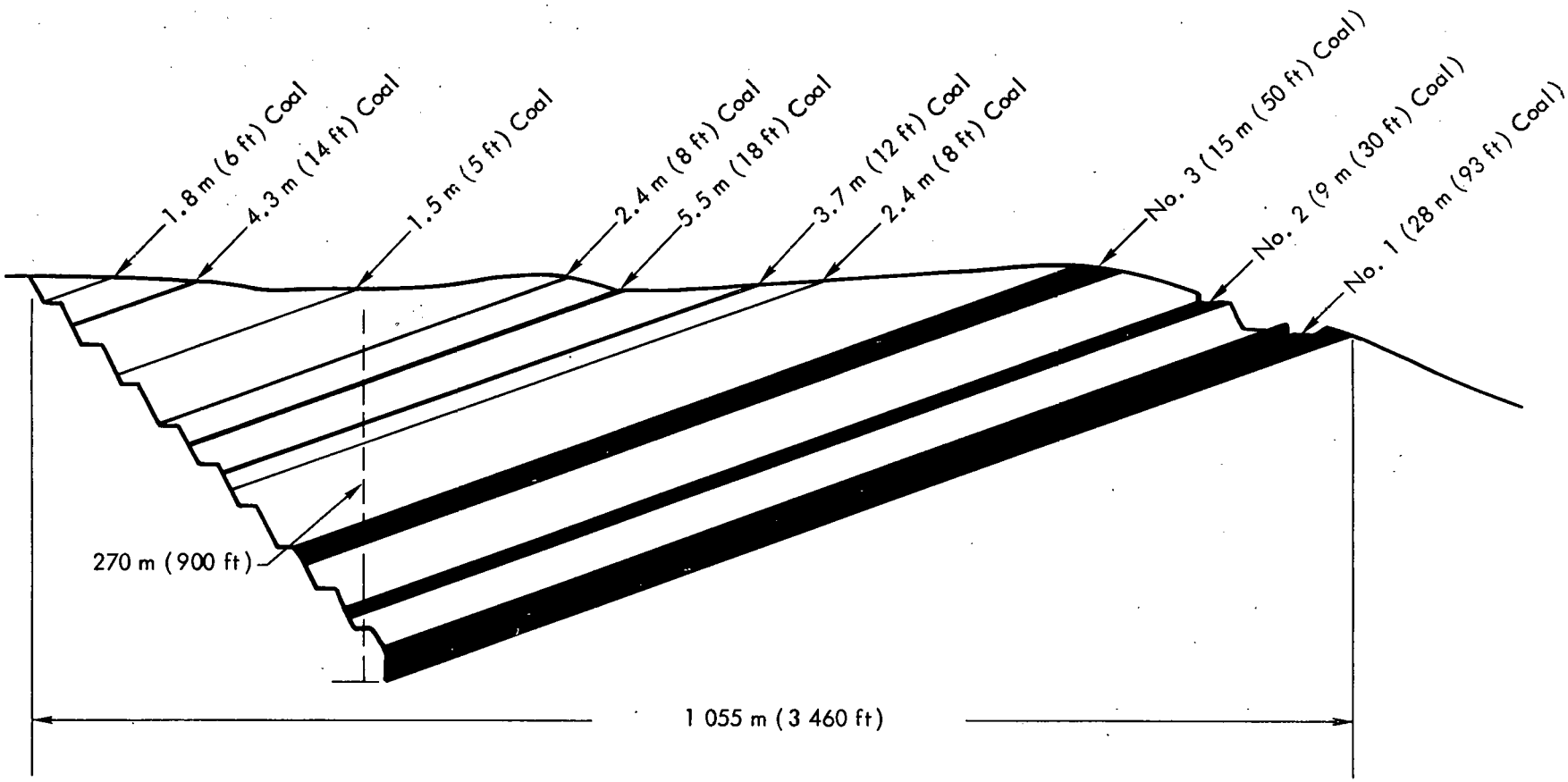

Fig. 2. Cross section of the big pit, Kemmerer Coal Company (scale 1:4800 (1 in. = 400 ft)). The experimental site is located in the main seam of coal. Numerous other seams permeate the local region.

A number of significant observations were made:

1. Some field interpretation of data is feasible and is done routinely.
2. High-frequency propagation can provide good resolution; HF high-resolution propagation through 15 m (50 ft) or more of water-saturated coal has been achieved easily.
3. Low-frequency measurements on the surface or in single or multiple drill holes can provide good resolution.
4. The permeability of the medium possibly can be determined via electrical methods.
5. More refined data interpretation is feasible by means of sophisticated computer-based procedures for data reduction.

Results are presented in this report that substantiate these claims. In addition, we present results specific to the Kemmerer site obtained from field interpretation and from more refined data interpretation. Also given are suggestions for future work, specific recommendations with respect to site selection and evaluation, data-collection procedures, new experimental techniques, and other possible applications of electrical methods.

POINT I: SOME FIELD INTERPRETATION OF DATA IS FEASIBLE AND IS DONE ROUTINELY

This point is perhaps best supported by four different findings.

1. The uniformity of the medium can be checked by HF techniques (subsurface) or LF techniques (surface and subsurface).

Either HF[1, 2] or LF[3, 4] techniques enable one to detect both lateral and depth variations in the region of interest.

HF techniques. An example of field interpretation of HF data for checking the uniformity of the medium is presented below for the situation depicted in Fig. 3. All the possible transmitter-receiver combinations for that situation were tried. These resulted in multiple paths linking transmitter and receiver and crossing the medium of interest. The dominant signal linking each transmitter-receiver pair is the signal traversing the direct-line path as depicted in the figure. Other modes (such as surface-reflected and up-over-down) are negligible compared to the direct mode, except very near strong electrical discontinuities (such as occur at the ground/air and coal/underburden interfaces).

If the medium is homogeneous (uniform), then the signal attenuation should be the same (1) for all horizontal paths, and (2) for all paths with a vertical separation of 3 m (10 ft), and so on. We now apply this test to the Kemmerer data.

Table 1 summarized the HF data taken for transmission between holes AR1 and AR3 (see Fig. 3 for a diagram of the transmission paths and see the Appendix for the data listings). For these two holes, the coal extends from the surface to a depth of somewhat more than 24 m (80 ft) but less than 27 m (90 ft). Thus, the horizontal

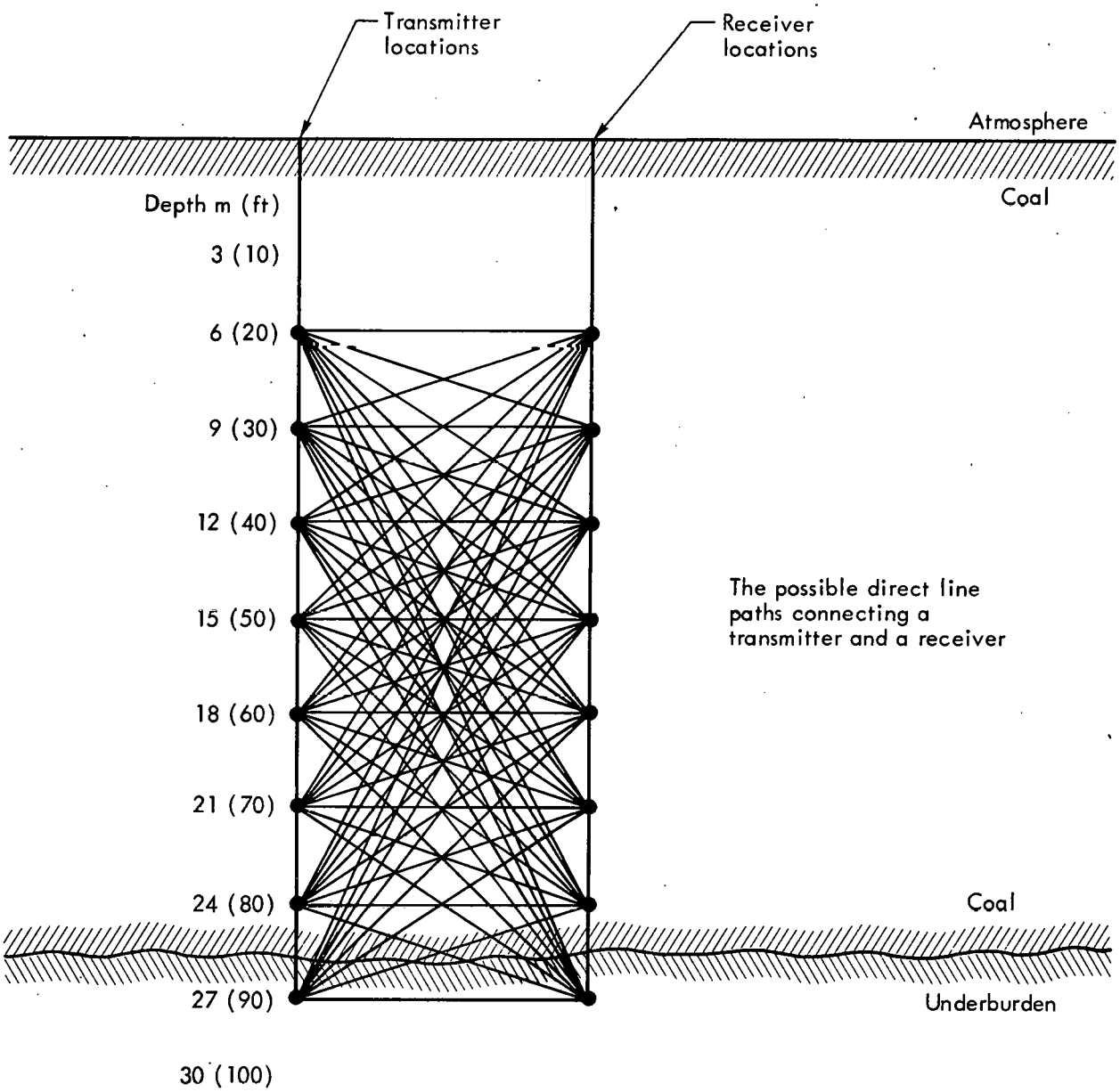

Fig. 3. Transmitter and receiver locations (depths in feet beneath the surface) for HF determinations of uniformity of the medium. Most sites were within the coal seam; a few were below the coal in the underburden. The direct-line paths are shown for all possible transmitter/receiver pairs.

Table 1. Amplitude data (in dBm) for transmission of 10-MHz signal between drill holes AR1 and AR3 at the Kemmerer site. The consistency of the hole-to-hole data was checked by comparing relative signal strengths for different paths of the same length (for example, the pathways from the transmitter at the 15-m (50-ft) depth to the receiver at the 12-m (40-ft) level and to the receiver at the 18-m (60-ft) level.

Transmitter depth (m (ft))	Receiver depth relative to transmitter depth (m (ft))						
	Same	+3.0 (+10)	-3.0 (-10)	+6.1 (+20)	-6.1 (-20)	+9.1 (+30)	-9.1 (-30)
6.1 (20)	-45	-49		-52		-60	
9.1 (30)	-48	-48	-50	-54		-62	
12 (40)	-49	-50	-49	-56	-55	-60	
15 (50)	-49	-50	-51	-56	-56	-61	-63
18 (60)	-49	-49	-53	-53	-59	-65	-63
21 (70)	-48	-48	-53	-61	-60	-76	-66
24 (80)	-47	-57	-51	-71	-56		-65
27 (90)	-60	-74	-53		-59		-66
Av [a]	-48.6	-49.25	-51.5	-55.33	-58.33	-61	-63
		-50.375		-58.83		-62	

[a] Averages of bracketed values, which exclude those outside the 30 to 70 range. Above 25 ft, there was a possibility that a transmitter or receiver might be above the water table, below 75 ft that either the transmitter or receiver might be in the underburden. Inside these limits, the medium was expected to be uniform.

transmission loss should be reasonably constant for equal transmitter/receiver depths between 6 m (20 ft) and 24 m (80 ft). This is seen to be approximately true for the horizontal data given in Table 1: note that when both transmitter and receiver are in the underburden (27 m (90 ft)), the attenuation is much more pronounced than when both are in the coal. Thus, the horizontal HF transmission definitely indicates the change in the subsurface medium. Any electrically significant anomalies (e.g., clay deposits, caverns, voids, dipping beds) between the two drill holes would be evident in these data.

The consistency of the medium can be further checked by measuring HF transmission for slanting paths. The slanting-path data for transmitter-receiver pairs with vertical separations of 3 m (10 ft), 6 m (20 ft), and 9 m (30 ft) are also given in Table 1. The essential uniformity of these results for paths in the coal further verifies the uniformity of the medium. The presence of underburden for either a transmitter or a receiver at a depth of 27 m (90 ft) is also readily apparent in the HF slanting-path data.

LF Techniques. Low-frequency surface measurements enable one to detect both lateral and depth anomalies.[3,4] Data taken with a fixed geometric spacing between four probes and with the center of the array being moved enables one to detect lateral variations. An example of this is the data shown in Fig. 4, where the variations are not dramatic but are indicative of a reasonably uniform subsurface to the depths probed. It is useful to mention an effective rule of thumb – that, for a uniform ground, the effective probing depth is of the order of one-third to one-half the total length of the array. That is to say, the longer the total length of the array, the greater the effective probing depth.

Besides LF surface and HF subsurface measurements, LF subsurface measurements can be used to determine the uniformity of the medium. A notable example of this is the downhole resistivity log produced by a commercially available system that yields LF resistivity vs hole depth. A log derived via this method is depicted in Fig. 5. Note the uniformity of resistivity at the coal and in the overburden. Also note the rapid change in resistivity at the coal/overburden interface, which presents a definite sharp electrical discontinuity.

A disadvantage of the resistivity log (which is the product effectively of four probes downhole) is that its effective radius is limited to the vicinity of the drill hole in which it is emplaced. Thus, subsurface anomalies between two drill holes may not be "seen" by the resistivity log. This difficulty can be overcome by using probes in two different holes or by using probes on the surface and in a drill hole. Then, the current paths linking the transmitter probes to the receiver probes must pass between the two holes, or from the surface to the hole, and this can increase interactions with anomalies. Some possible probe configurations are shown in Fig. 6. This method with two drill holes was used at Kemmerer; the good fit of theory to experiment (see Figs. 7 and 8 for examples) for numerous transmitter and receiver locations (the receiver locations are the same as the HF receiver locations in Fig. 3) indicated a reasonably uniform medium between the drill holes.

2. General site surveys can be conducted via electrical methods at relatively low expense before deciding on relatively expensive detailed studies.

The degree of uniformity of a site can be ascertained by means of the surface and subsurface electrical methods described above. If the site meets the necessary constraints, such as freedom from caverns (this was a worry at Kemmerer) or anomalies (e.g., clay pockets), than more detailed experimental techniques can be fielded with confidence.

3. The porosity of the medium can be ascertained from in-situ measurements of a large volume of material.

Porosity can be measured on samples of the medium, but a question always remains as to how well a sample (or a number of samples) truly represents the bulk properties of the medium. By taking surface four-probe resistivity measurements (which yield the resistivity of a large volume of material), and then measuring the resistivity of the water in the medium (taken from a drill hole first pumped out and then

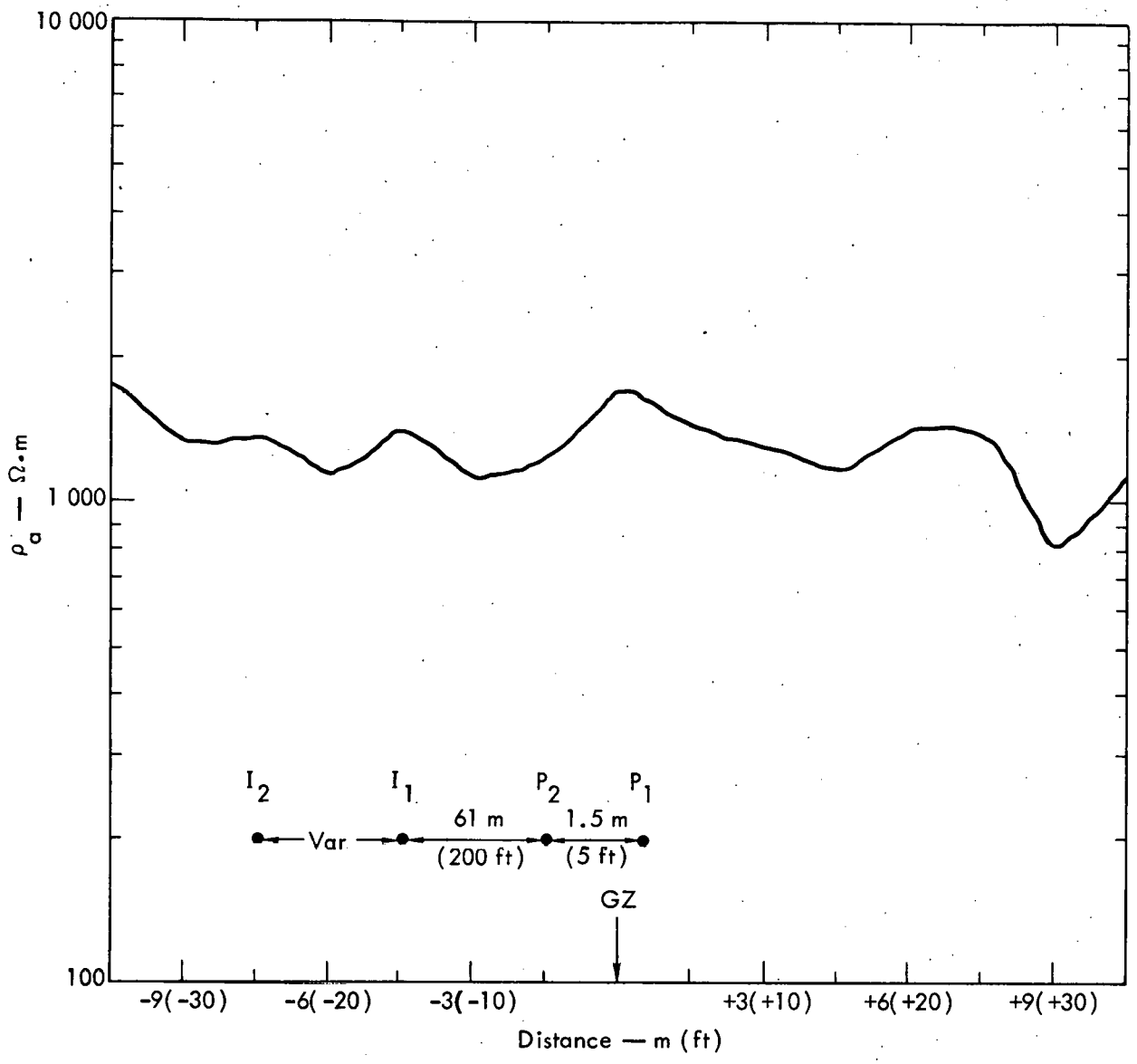

Fig. 4. Horizontal profile (apparent resistivity ρ_a) in coal along a north-south line extending 10.7 m (35 ft) in each direction from the center point (GZ). The center of the probe array was varied as indicated by the distances on the abscissa, but a fixed geometric separation was maintained between the probes. In this way one can detect lateral variations. By varying the total length of the array, one can vary the effective depth of probing. Thus, both lateral and depth variations can be detected.

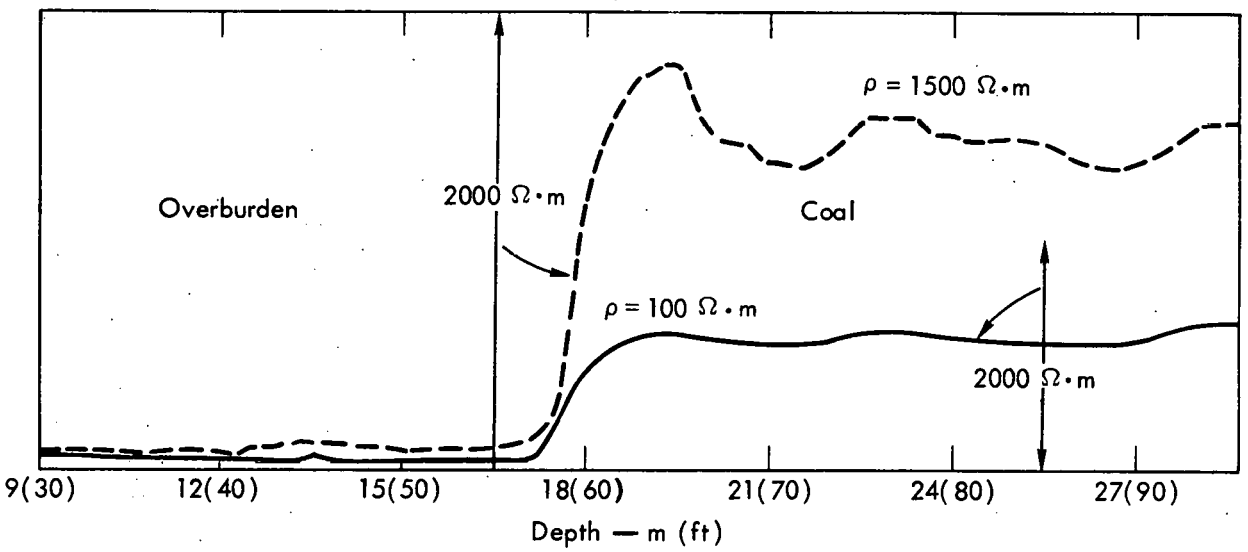

Fig. 5. Single-hole resistivity log. This provides information on the variation of resistivity vs depth. This resistivity profile is not for the region near the shot hole; it was taken on the other side of the strike from the shot hole, i.e., what is at the surface for the electrical-profile hole is overburden (clay), not coal as is the case for the shot hole.

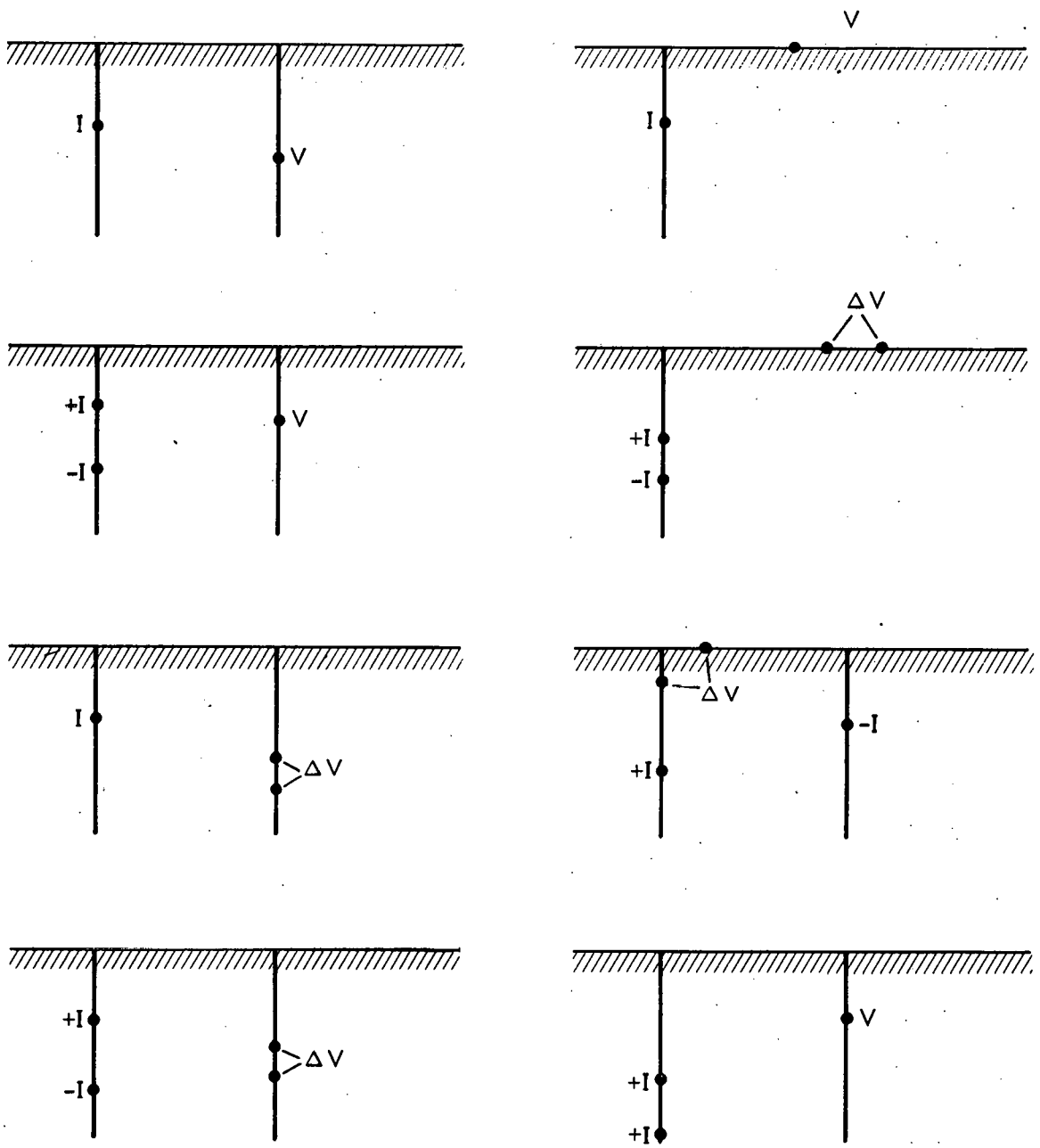

Fig. 6. Possible transmitter/receiver probe configurations that can be used to discern subsurface anomalies in the near vicinity of multiple drill holes.

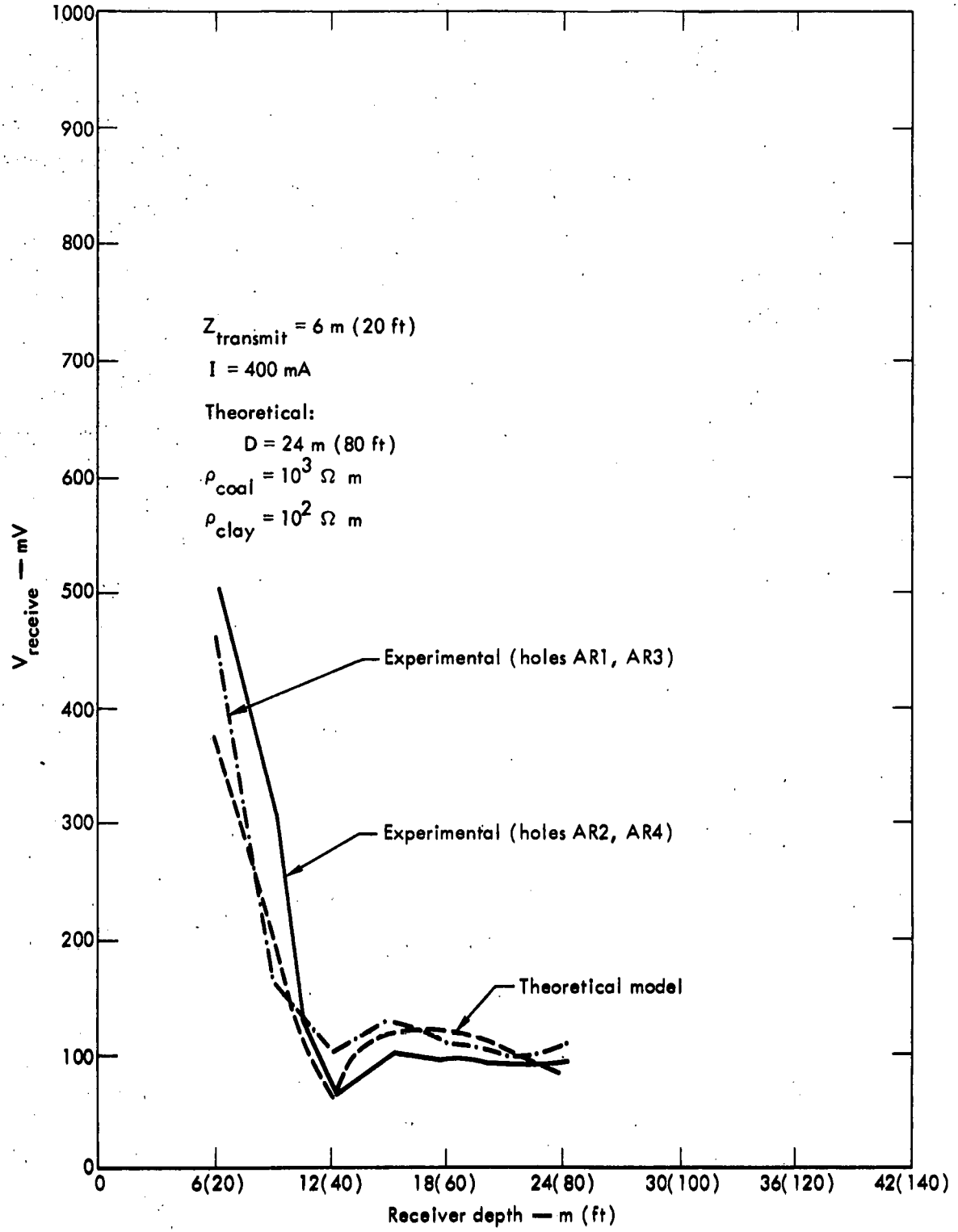

Fig. 7. Results from LF equatorial-dipole array with a pair of transmitter probes centered about a depth of 18 m (60 ft). This plot of V_{rec} (the difference in potential between the two receiver probes) vs receiver depth shows that for a uniform layer the experimental response compares well with the theoretical for a range of receiver locations. $Z_{transmit}$ = depth of center line of transmitter array; $Z_{receive}$ = depth of center line for receiver array; D = thickness of coal seam; ρ = resistivity.

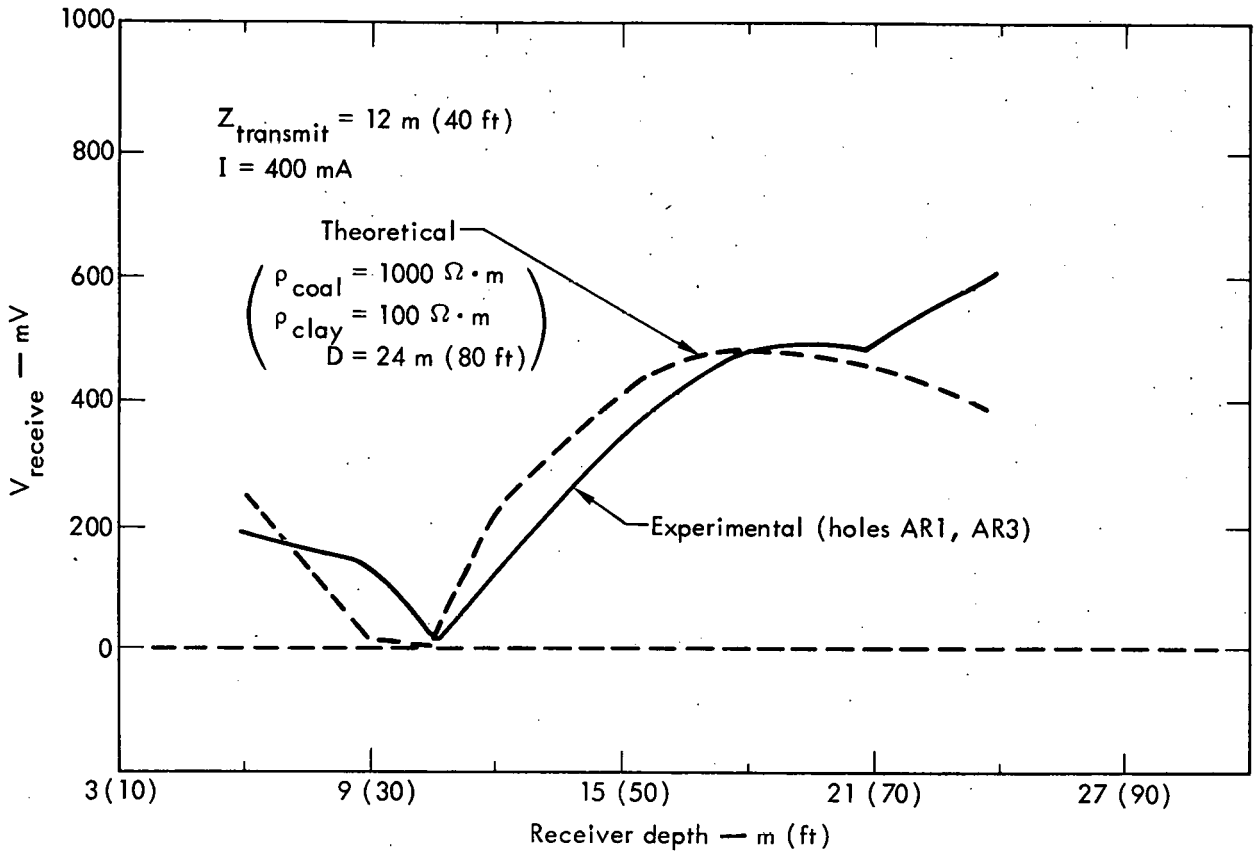

Fig. 8. Results from LF monopole-dipole array. With a single transmitter probe located at a depth of 6 m (20 ft), the comparison between the experimental response and the theoretical response for a uniform layer of coal is good, as shown for a range of receiver locations.

allowed to fill), one can easily estimate via Archie's Law[3] the porosity of large volumes of the medium. This was done at the Kemmerer site; the result for the porosity of coal was 6.3%.

4. Bad or questionable data points can be identified and checked.

The simplicity and relative ease of interpretation of the electrical methods (at least for reasonably uncomplicated subsurface conditions) permit ready detection of "bad" data points in the field. In any field operation, the conditions peculiar to each site and to the experimental method inevitably lead to some bad data (erroneous readings via a valid experimental procedure). Depending upon the data-reduction algorithm, such an erroneous datum can significantly affect the experimental conclusion. If the trend of the data and its significance can be discerned in the field, the obviously bad data points can be identified there and the erroneous reading can be corrected at little expense. When obviously erroneous readings are detected after leaving the field, the suspected data sometimes are not rechecked; certainly rechecking at that point is more costly than rechecking before leaving the field.

POINT II: HF PROPAGATION CAN PROVIDE GOOD RESOLUTION

This point can be demonstrated by three observations.

1. Transmission of HF signals through 15 m (50 ft) or more of water-saturated coal was achieved at Kemmerer.

This was done with a low-level (~5 W) power incident upon the transmitting antenna, a short nonresonant transmit antenna (leading to poor coupling efficiency of incident power into actual transmit power), and a short receiving probe. Data were recorded in some cases for frequencies of 1 to 100 MHz. An example of the data taken around the first shot hole is given in Fig. 9 for frequencies of 1 to 51 MHz; both absolute amplitude and relative phase shift were recorded. This was done for numerous combinations of transmitter and receiver locations in two separate drill holes (see Fig. 3 for the combinations tried). Longer transmission distances could be achieved through either a more efficient antenna system or a higher transmit power; such modifications are feasible.

2. Good resolution is attainable with HF transmission.

This is possible because of two different effects. One effect is that for HF, the wavelength at 50 MHz in the Kemmerer coal is 1.5 m (the relative dielectric constant is approximately 16, which slows electromagnetic wave propagation by a factor of 4 relative to free space). This enables one to discern interference phenomena over reasonably small distances. The second effect is that the HF propagation can be accurately modeled by the use of ray optics. Thus, gross volume effects that may change only slowly about the direct line linking the transmitter to the receiver do not significantly affect the transmission. This means that if a direct ray path intercepts some electrically significant anomaly, its effect will be noted. If there are electrically significant anomalies near the direct path, then swept-frequency excitations will

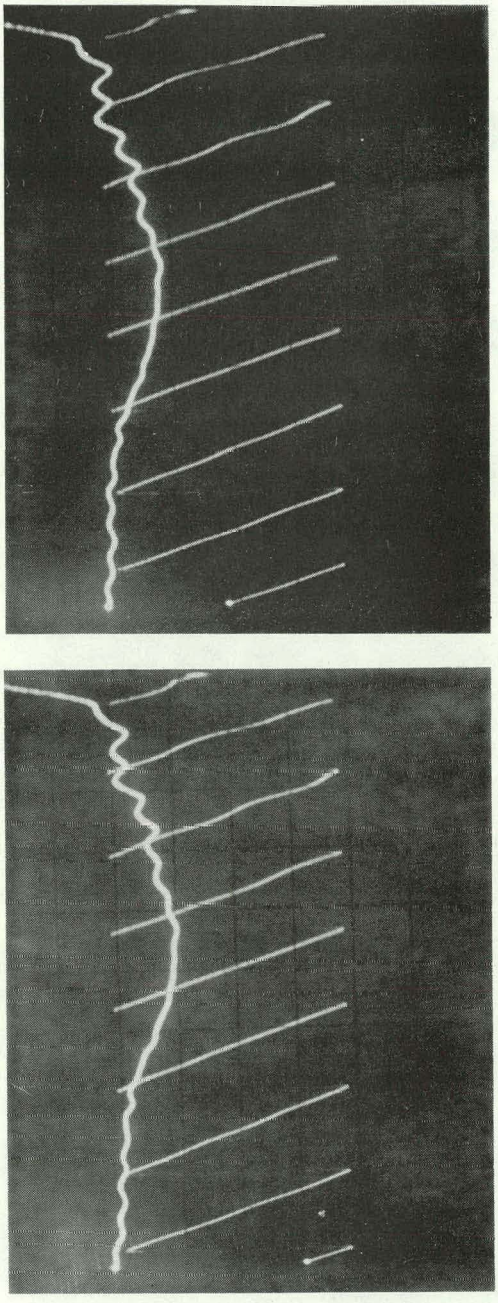

Fig. 9. Transmission of HF signals through coal. The relative magnitude and phase of the response for various transmission paths can be compared to discern the uniformity of the medium. The curve represents amplitude data and the diagonal lines represent relative phase shift.

identify this situation by the characteristic variation in interference pattern with frequency. An example of the effect (obtained at a site in limestone[2]) is shown in Fig. 10. This procedure for coal will be discussed in more detail in the postshot report.

3. HF propagation operates well even if there are voids.

A number of situations arise where there are voids in the ground. These may be either man-made (e.g., mined areas, or spaces left after in situ coal gasification) or natural (e.g., gas caverns or eroded regions). High-frequency waves propagate via displacement currents, not conduction currents; thus, they move as well through voids, as they do through water or rock. Thus, the limitations imposed by air spaces (electrically and acoustically nonconducting) upon LF electromagnetic and seismic methods do not inhibit HF electromagnetic methods.

POINT III: LF MEASUREMENTS CAN PROVIDE GOOD RESOLUTION

This point can be illustrated by four observations.

1. The coal-bed region is accurately defined by well logs.

The coal/underburden interface has been well defined by measurements in a single drill hole. The electrical log (see Fig. 5) indicates a definite sharp discontinuity at the same depth as do the density log (see Fig. 11) and the three-dimensional velocity log (see Fig. 12). In addition, the electrical log[3] (and also the density and three-dimensional log) indicates a reasonably uniform coal bed; no large-scale anomalies (jumps in resistivity) occur. This is completely unlike the results commonly encountered with resistivity logs at the Nevada Test Site. From Fig. 5 it is seen that for LF excitation, a nominal underburden resistivity is $\rho_u = 100\ \Omega \cdot m$ and a nominal coal resistivity is $\rho_c = 1500\ \Omega \cdot m$. This value for coal is in close agreement with the geometric average ($\rho_c = 1570\ \Omega \cdot m$) of the LLL core-sample results (based upon core sample results of $\rho_c = 790\ \Omega \cdot m$ and $\rho_c = 3130\ \Omega \cdot m$).

One difficulty with single-drill-hole measurements is that the effective radius of probing is limited to the near vicinity of the hole. Thus, alternative methods must be used to sample the larger volumes of interest. These limitations may be overcome by probing from the surface, probing from multiple drill holes, and combinations of surface and drill-hole probing.

2. Multiple-drill-hole probing provides good resolution.

Two downhole probe configurations were used at Kemmerer: the equatorial dipole and the monopole-dipole (see Fig. 6). A large number of transmitter locations and receiver locations was used (those shown in Fig. 3) to ascertain whether the coal bed contained any subsurface anomalies. One might think that LF data would have no resolving power at all, since the wavelength at the excitation frequency of 20 Hz is 15 000 km. However, by taking data at many physical locations, one can effectively use geometric positioning to overcome some of the difficulties arising from wavelength dimension. This fact is well known for surface four-probe surveys. Here we apply the same idea to subsurface surveys. The preshot measurements do not indicate any

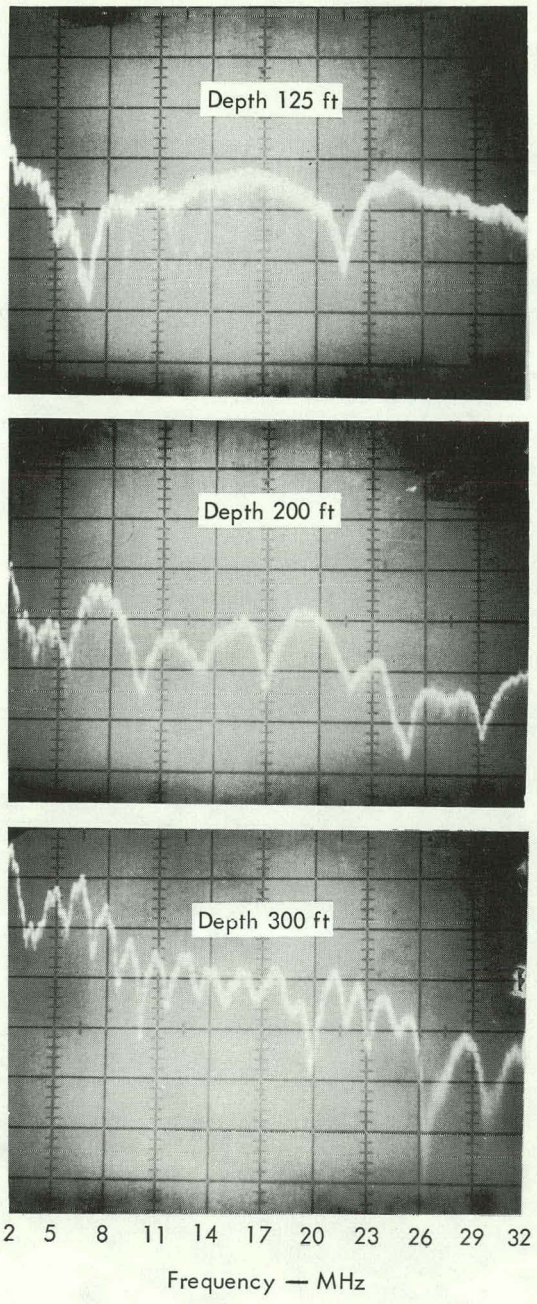

Fig. 10. Swept-frequency-transmitted signals for transmitter/receiver depths of 38 m (125 ft), 6. m (200 ft), and 168 m (550 ft). Direct rays and those reflected from subsurface anomalies can constructively and destructively interfere, leading to notching behavior with frequency. The width of the notch is directly related to the distance to the anomaly.

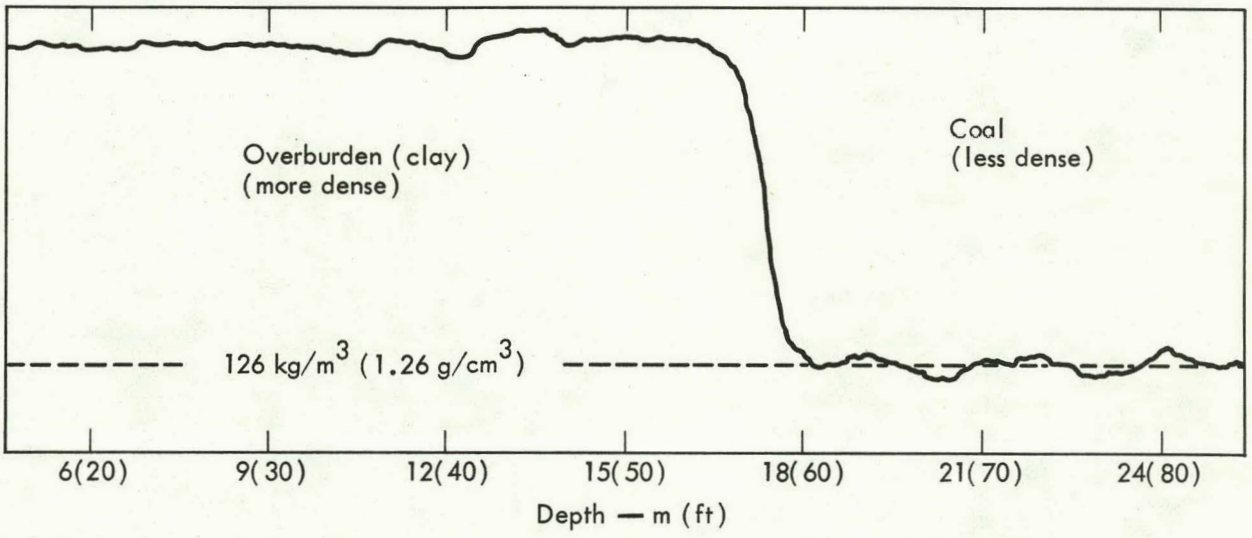

Fig. 11. An LF well log from a drill hole near the shot hole showing very uniform densities for the coal and for the clay. The curve indicates a sharp change in density at the clay/coal interface. This drill hole is the one for which the resistivity log is given in Fig. 5; hence, clay overburden and not coal is at the surface. Compare also with the three-dimensional velocity log for the same drill hole in Fig. 12.

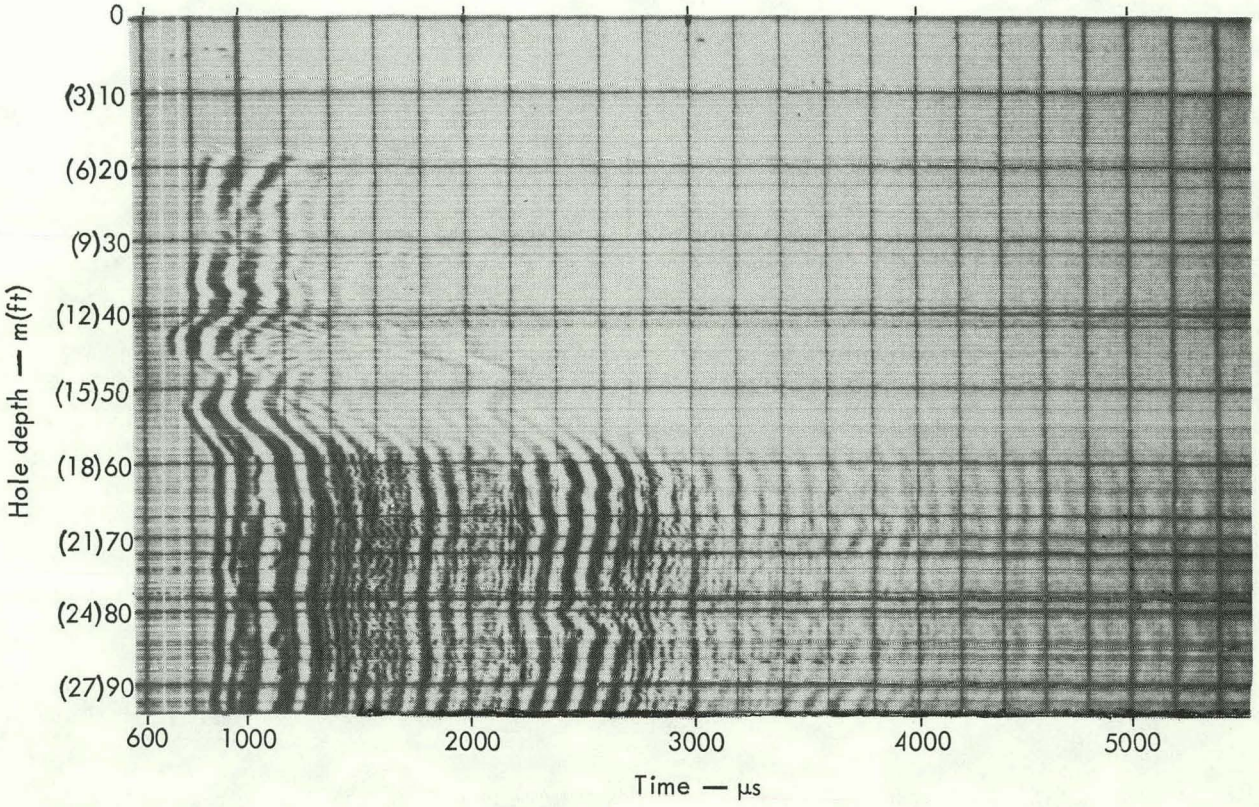

Fig. 12. A three-dimensional velocity log. The acoustic transmission characteristics of the clay and the coal are decidedly different. These acoustic velocity data (for the same drill hole as in Figs. 5 and 12) indicate a sharp discontinuity at the coal/clay interface.

large anomaly. In fact, the match between the experimental measurements and the theoretical results for a medium composed of several homogeneous layers is good. Examples of the degree of match are given in Fig. 7 for the equatorial dipole configuration and in Fig. 8 for the monopole-dipole configuration.

One can argue that an anomaly would distort the fields, but it would be prudent to demonstrate this by theoretically modeling this situation for the probe configurations used, and also to perform scale-model laboratory experiments. The theoretical problems can be solved by using either finite difference equations or probabilistic potential theory. A facility for scale-model laboratory work is being built at LLL for the study of problems of this kind. The multiple-drill-hole results indicate not only the depth and the resistivity of the coal and the resistivity of the underburden (as did the electrical log), but they also indicate the volume electrical uniformity of the coal bed.

3. Surface probing helps to define the subsurface profile.

The four-probe LF surface probe picks up lateral variations when the geometric positions are fixed but the center of the array is moved. Figure 4 gives an example of this with the array located 9 m (30 ft) into the coal bed parallel to the strike. A second way of probing combining depth and lateral effects is illustrated by example in Fig. 13. This depicts the extent of the anomalies[3, 5] on the overburden side of the strike. This surface probing was designed to detect the presence of suspected caverns; several suspicious locations were identified but drilling at these locations revealed no caverns. This combination of surface probing with drilling at suspicious areas ensures that in situ coal fracturization shots will be performed only in clearly identified uniform areas. This is a wise expenditure of time and money. For, example, many holes might be drilled in a search for caverns, but if suspicious areas were identified previously, the number of drill holes could be decreased and the level of confidence about the subsurface conditions could be raised.

The variation of resistivity with depth can also be ascertained, as shown by the example in Fig. 14. The shallow penetration (for an array over the coal seam) gives a high resistivity characteristic of coal. As depth of penetration increases, resistivity decreases. This decrease is especially rapid for total array length greater than 61 m (200 ft), where the penetration of the current is such that a significant portion travels through the underburden beneath the coal. This underburden has a resistivity of about 100 $\Omega \cdot m$; the surface resistivity asympotically approaches it. This is characteristic of a two-layer earth (coal with clay underburden). Thus, general subsurface features can be identified in this way from the surface.

An even more striking example of the degree of resolution of LF surface profiling is that the dip angle of the coal seam can be identified as 18 deg from surface resistivity soundings taken perpendicular to the strike (Fig. 15). The data-reduction procedures leading to this conclusion are perhaps better explained elsewhere; the interested reader is referred to Ref. 3 for a clear exposition.

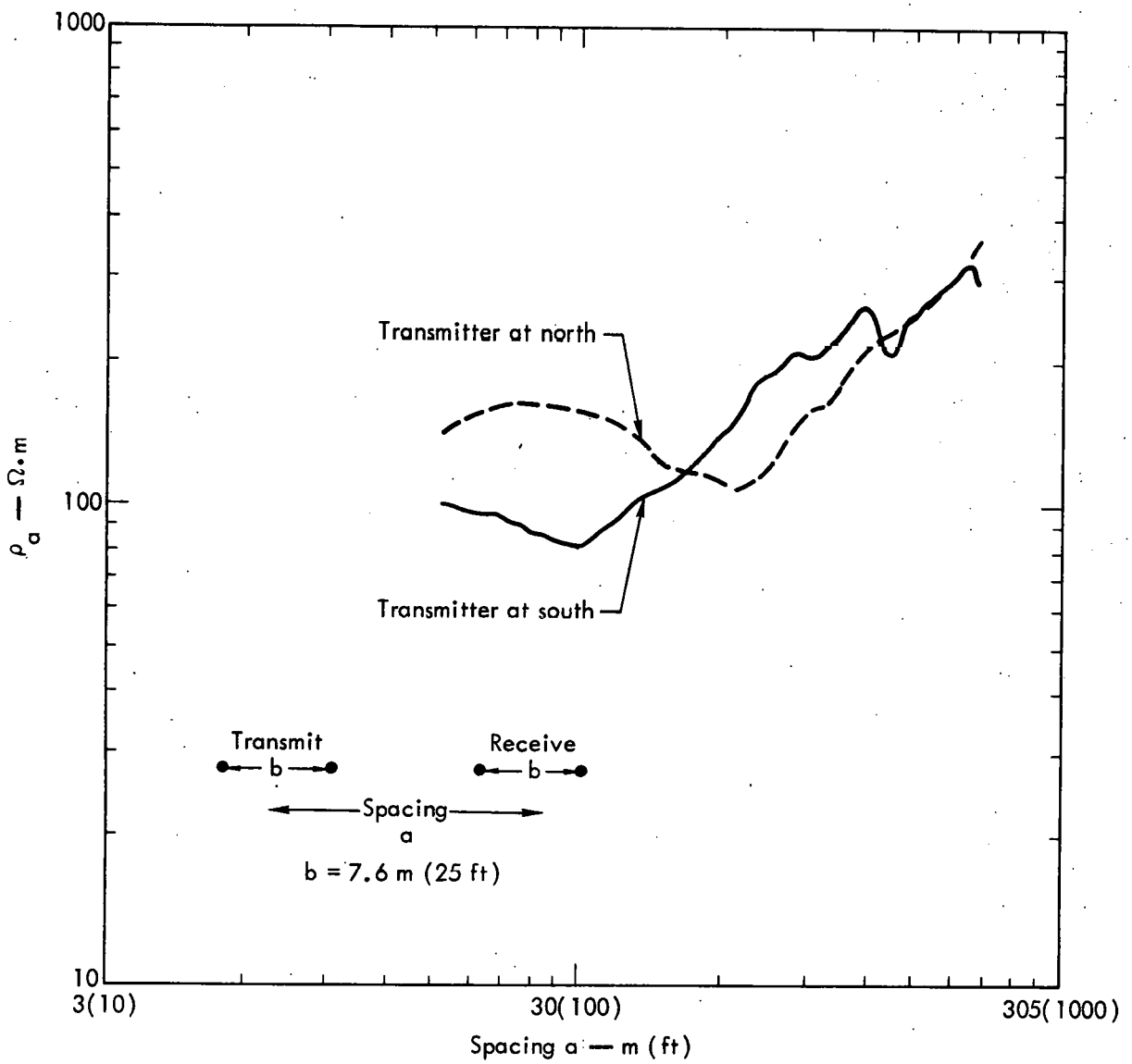

Fig. 13. Apparent resistivity ρ_a vs "spacing a" (defined in the figure) for a dipole-dipole array in overburden. Surface profiles combining depth and lateral information can be used to detect possible large caverns. This was tried at Kemmerer along two lines parallel to the strike and located over the overburden. The first (transmitter at north) was run for various receiver locations in a southern direction. The second (transmitter at south) was run for various receiver locations in a northern direction.

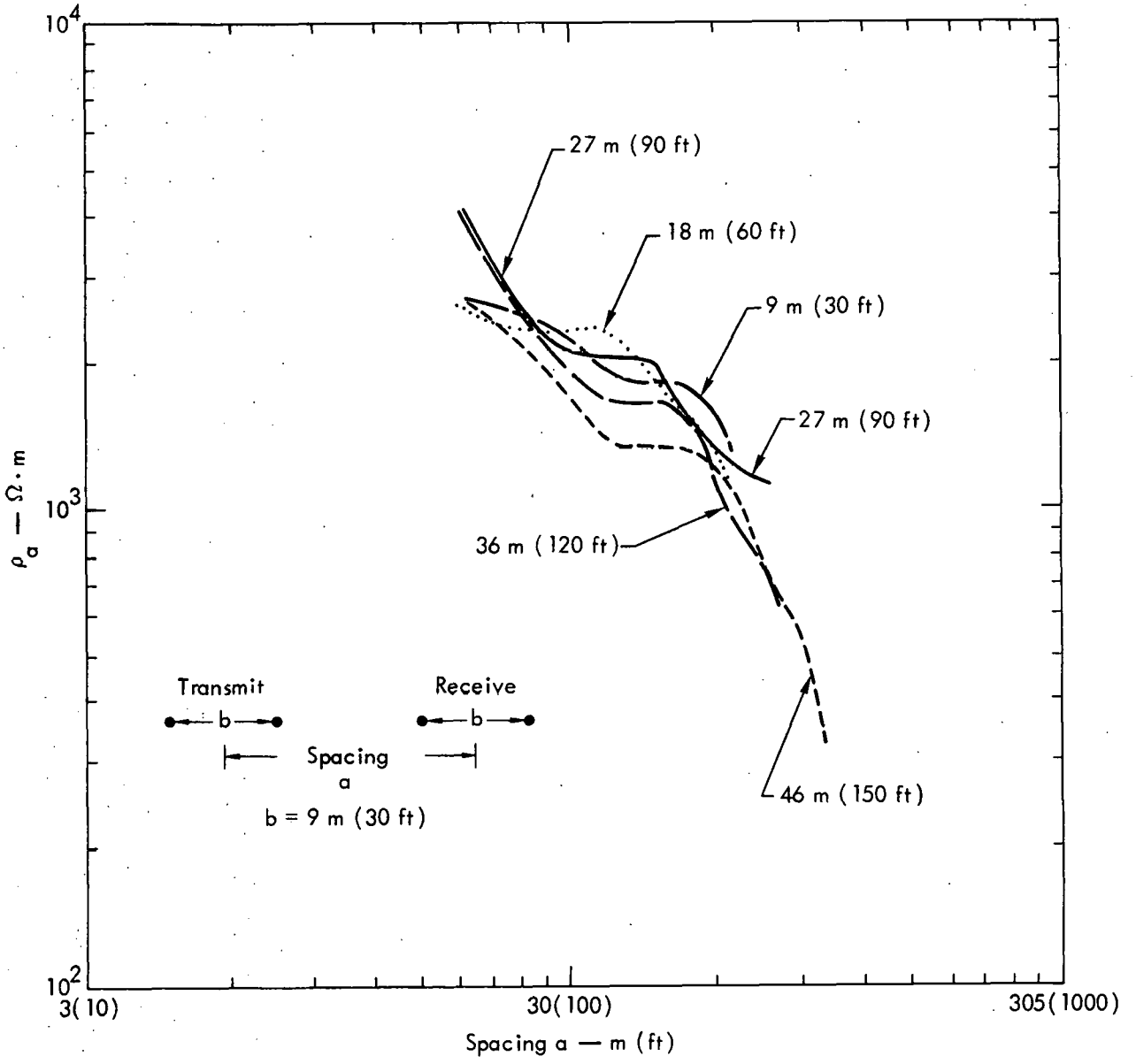

Fig. 14. Apparent resistivity ρ_a vs "spacing a" for a dipole-dipole array in coal. The dipole lengths were 9 m (30 ft). The curves are for different distances (as indicated on each curve) between I_1 and GZ. The effective depth of probing is related to the length of the array. With the center point of the array remaining fixed over GZ, the length of the array was varied to obtain a depth profile. The curves are for different distances (as indicated) between I_1 and GZ.

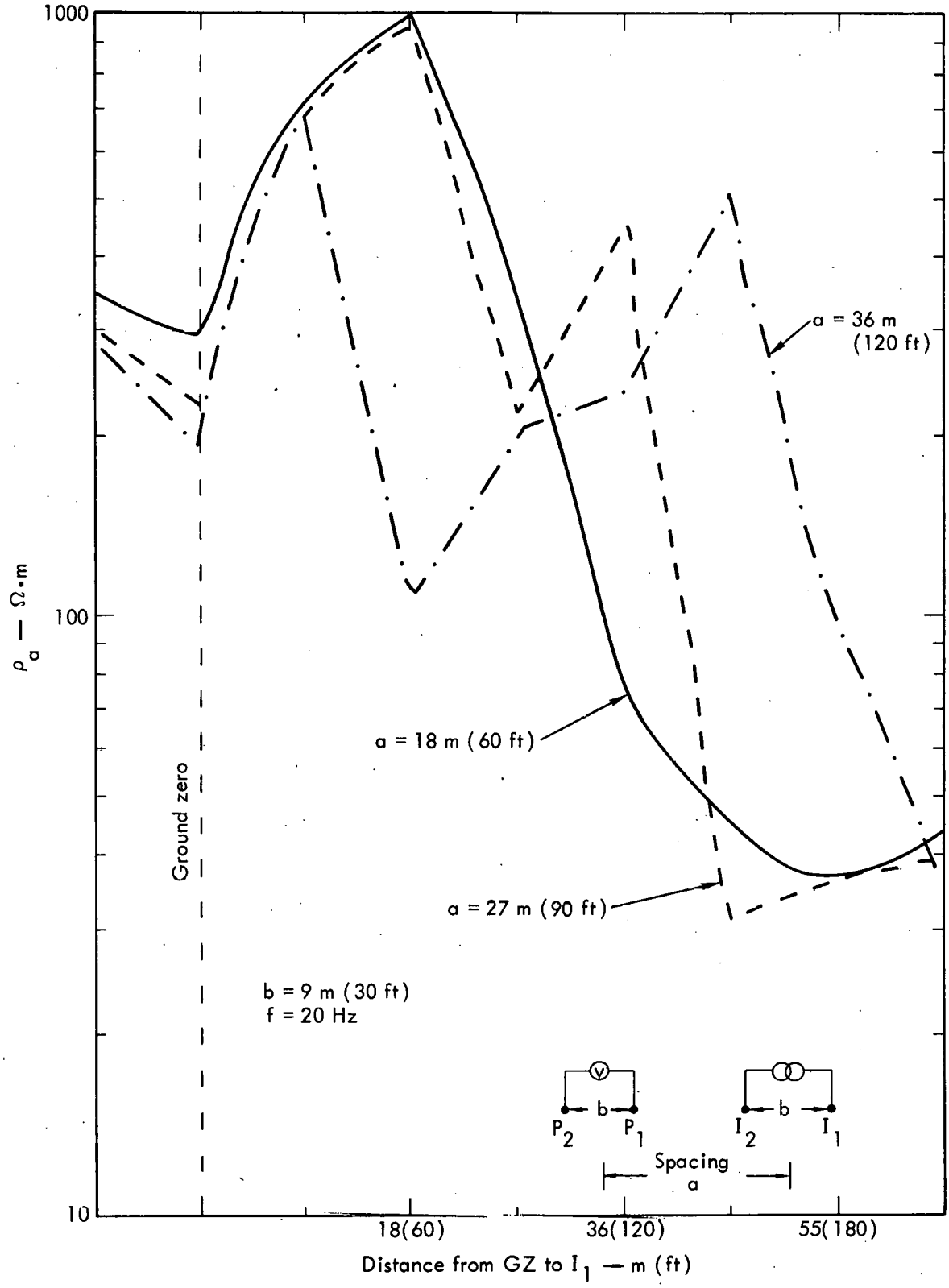

Fig. 15. Three different dipole-dipole resistivity profiles taken perpendicular to the strike and indicating the dip angle of the coal bed. In all three, "spacing a" was either 18 m (60 ft), 27 m (90 ft), or 36 m (120 ft).

It is worth noting that the Kemmerer work included an effort to determine the usefulness of frequency effects with four-probe measurements. The four-probe scheme was tried for frequencies of 20 Hz (the usual operation frequency), 100 Hz, 200 Hz, 1 kHz, 2 kHz, and 10 kHz. The resistivity results for a fixed probe location were essentially the same for all frequencies. Thus, there was no apparent advantage in using a higher-frequency excitation than 20 Hz for four-probe measurements.

POINT IV. IT MAY BE POSSIBLE TO DETERMINE PERMEABILITY IN SITU VIA ELECTRICAL MEASUREMENTS

A recent suggestion by both J. L. Cramer[6] and A. G. Duba[7] opens up a new approach to the in situ determination of permeability. Both pointed out that if the resistivity of the medium were altered by the injection of a saline solution, then it might be possible to determine the permeability in situ by electrical methods. The electrical methods proposed do not measure permeability directly; rather, they measure the velocity of a pressurized fluid pulse as it moves through the medium. Our conversations with J. H. Pitts[8] indicate that in situ differential pressure measurements and velocity measurements could be used to determine the permeability.

It should be stressed that what is desired is a change in the in situ resistivity as the fluid pulse propagates. This can be accomplished either with a saline solution as mentioned above, or with a fluid of lower conductivity than occurs naturally in the medium.

The measured resistivity of the bulk-water-saturated coal at Kemmerer is 1500 $\Omega \cdot m$, and that of the water from a downhole sample 1210 $\Omega \cdot m$. If a saline solution changes the resistivity of the water to 1 $\Omega \cdot m$ (a 10:1 charge), then the new bulk resistivity would be approximately 150 $\Omega \cdot m$.

It is acknowledged, of course, that not all of the pore spaces indicated by this calculation are connected; hence, the bulk resistivity only approached 150 $\Omega \cdot m$; i.e., it is not precisely 150 $\Omega \cdot m$.

Electrical methods have the potential of monitoring the velocity in a three-dimensional sense (i.e., at the locations between drill holes) rather than measuring the average velocity between the two drill holes. This could enable us to determine permeability in the three-dimensional sense. Thus, problems of nonuniform flow like that depicted in Fig. 16 could be seen developing and accordingly interpreted. Present methods would not adequately model such situations. We recommend that electrical methods of measuring velocity in situ be tested to ascertain their usefulness. A simple experiment at the Kemmerer site would enable us to achieve this objective. The two methods described below are the ones which may yield three-dimensional velocity information.

Method 1. HF Hole-to-Hole Attenuation

Figure 17 depicts two geometries that can be used for an HF electromagnetic method. A single-frequency continuous-wave signal or a swept-frequency signal can

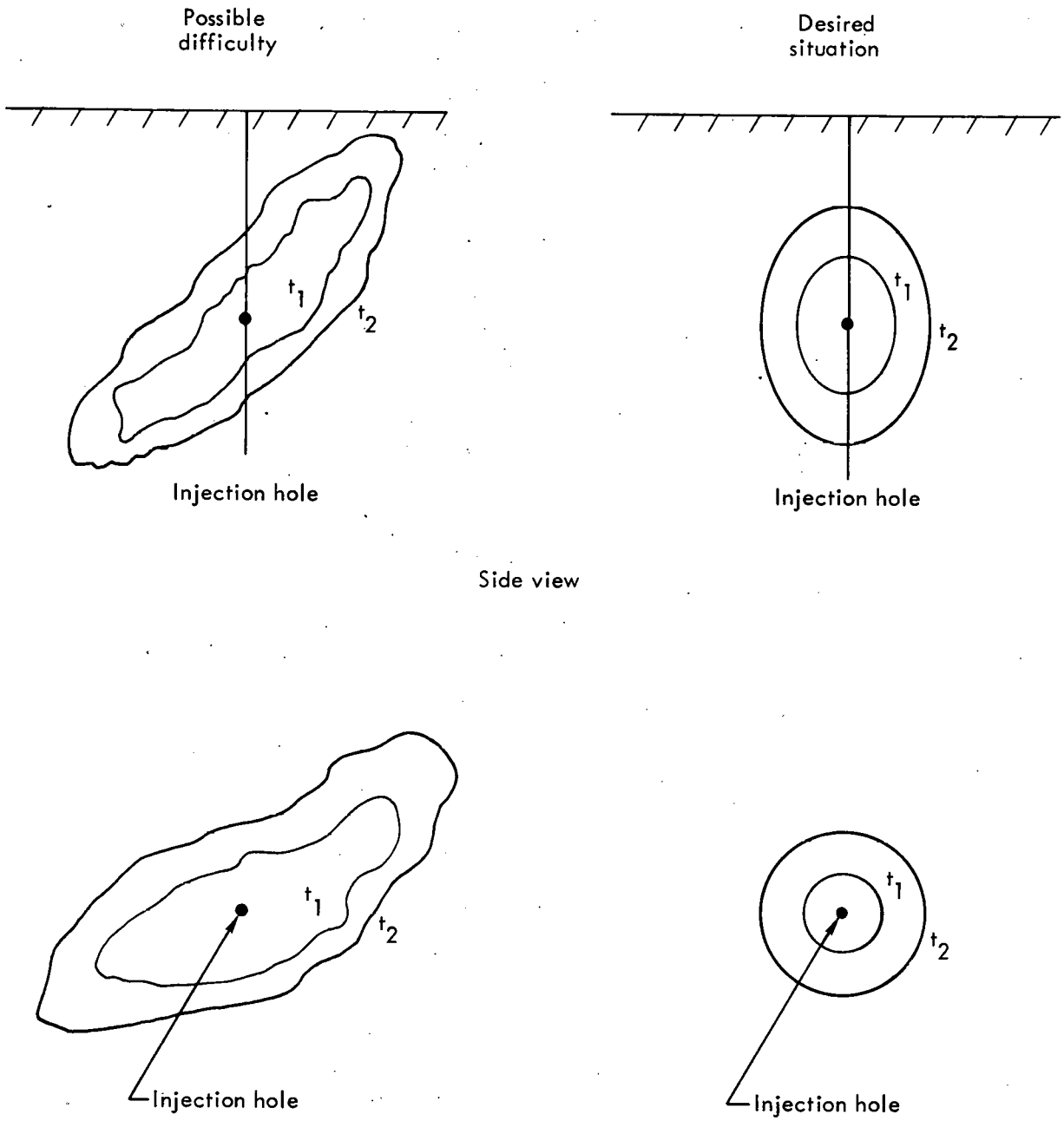

Fig. 16. Example showing how nonuniform pressure-induced fluid flow might be misinterpreted without the capability for three-dimensional monitoring of velocity (t_1, t_2, progressive times).

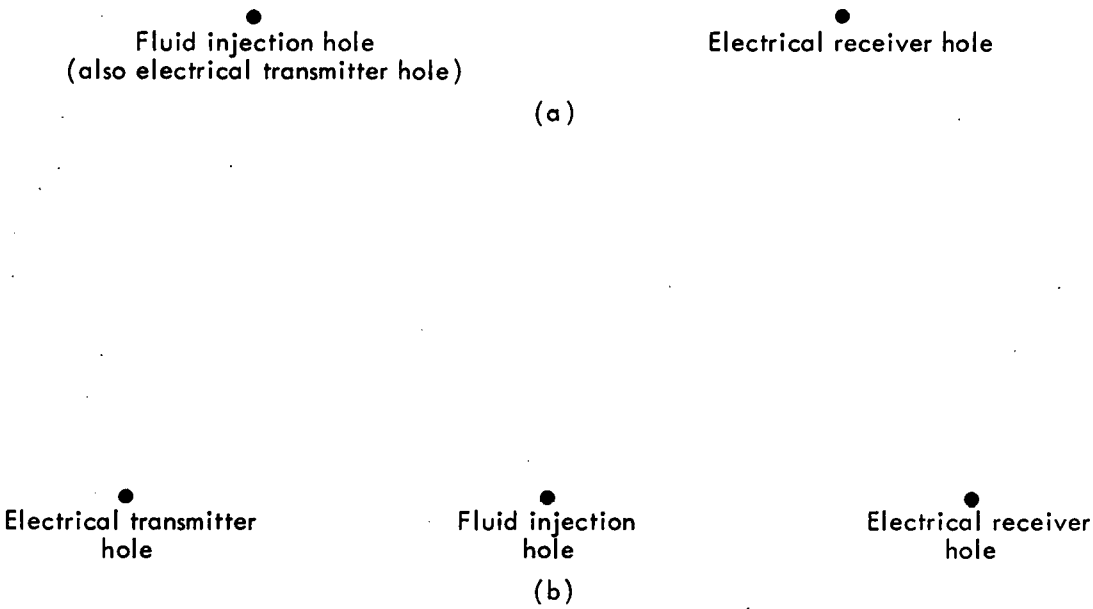

Fig. 17. Two possible test geometries for in-situ measurement of pressure-generated fluid velocity through the medium. From the attenuation characteristics one can determine the permeability. (a) Transmitter and fluid injection in the same hole; (b) transmitter and fluid in two different holes, avoiding a technical problem of locating the transmitter in the fluid injection hole.

be used. The amplitude of the received signal is noted on an oscilloscope and then the "unnatural conductivity fluid" is injected. As the fluid penetrates the surrounding medium, the bulk resistivity is modified and the received signal is altered. The velocity of the fluid expanding throughout the connected pore spaces of the medium can now be related to the time history of the attenuation curve.

Method 2. Interference phenomena

This method (Fig. 18) uses a transmitter and receiver in the same hole (see Fig. 2). The transmitter emits a signal which is reflected by the injected fluid. This reflected signal interferes with the direct signal that links the transmitter and the receiver. For swept-frequency excitation, this interference (constructive and destructive) causes "notching behavior" in the amplitude of the received signal. The width of the notches is related directly to the distance from the point of reflection. From this information one can follow the movement of the fluid front with time.

POINT V. SOPHISTICATED DATA INVERSION ALGORITHMS YIELD DETAILED SUBSURFACE PROFILES

1. The relative dielectric constant does not vary significantly.

The interpretation of HF data is based upon ray optics formulas for expressing the attenuation and phase shift of a signal passing directly between source and receiver. It is well known that the phase shift ϕ of a plane wave passing a distance R through a medium of relative dielectric constant ϵ_r is

$$\phi = \frac{\omega}{c} \sqrt{\epsilon_r}\ R,$$

where w is the frequency ($w = 2\pi f$) and c is the speed of light in free space. For a swept-frequency mode from frequency f_1 to f_2, the differential phase shift $\Delta\phi$ is

$$\Delta\phi = \phi(f_2) - \phi(f_1) = \frac{R}{c}\left[f_2\sqrt{\epsilon_r(f_2)} - f_1\sqrt{\epsilon_r(f_1)}\right].$$

If $f_2 \cong f_1$, then $\epsilon_r(f_2) \cong \epsilon_r(f_1) \cong \epsilon_r$. Thus,

$$\Delta\phi \cong \frac{R}{c}\sqrt{\epsilon_r}\,(f_2 - f_1).$$

To generalize this to a multi section path of varying thicknesses and varying ϵ_r (see Fig. 19), if the ϵ_r values do not change dramatically from point to point, then

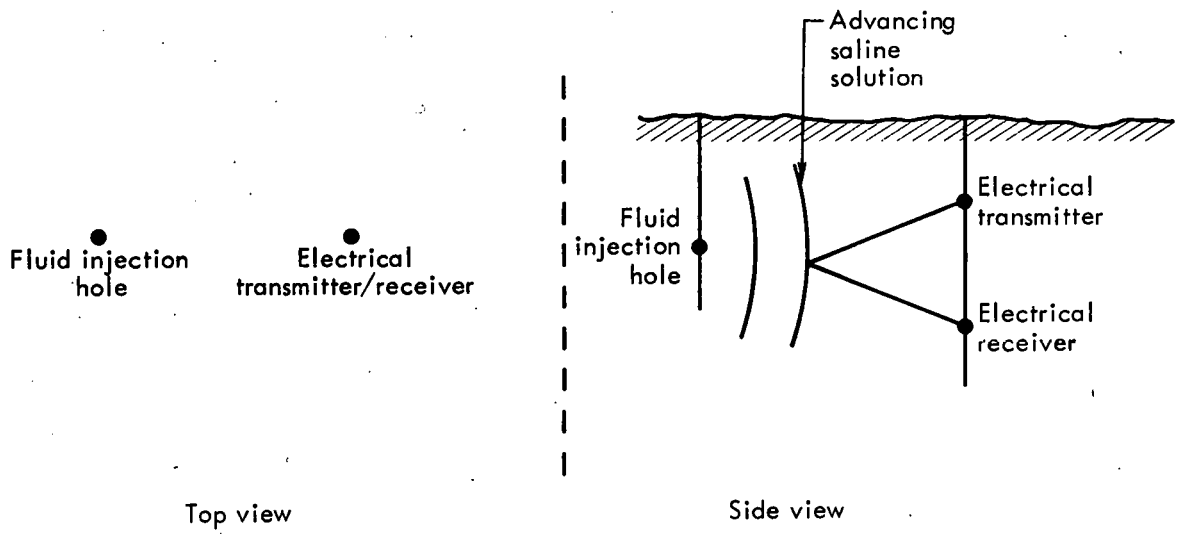

Fig. 18. Probe configuration for determining fluid velocity in situ by observing the change in the interference pattern as a function of time.

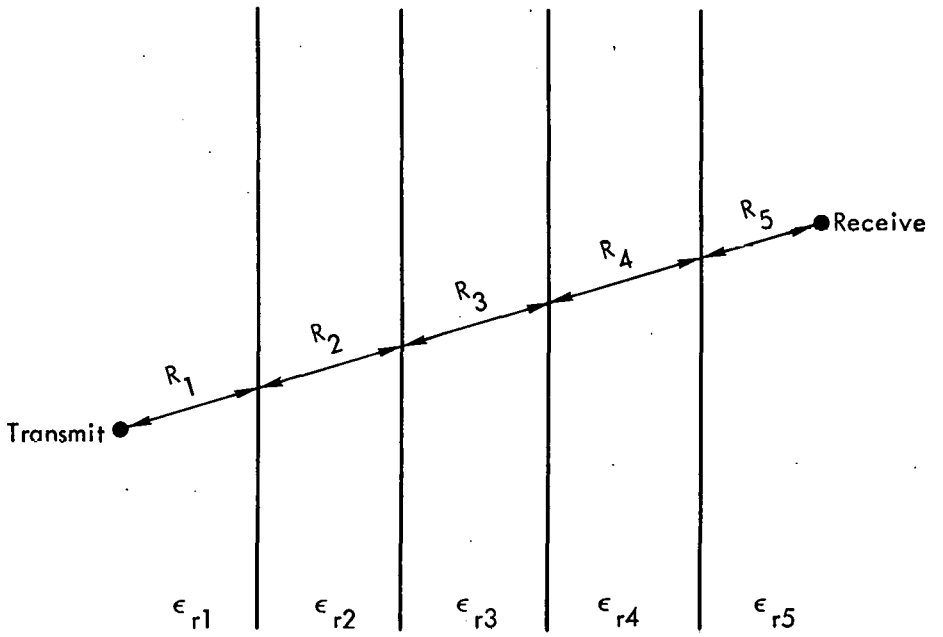

Fig. 19. Transmission through a smoothly varying multisectional path can be treated by considering separately the contributions of differential segments of the path.

$$\Delta\phi = \frac{(f_2 - f_1)}{c} \left[R_1\sqrt{\epsilon_{r1}} + R_2\sqrt{\epsilon_{r2}} + \cdots + R_N\sqrt{\epsilon_{rN}} \right] .$$

This formula was applied to the situation at Kemmerer to determine the ϵ_{ri} values for various subsurface models. Some preliminary estimates of ϵ_r values for different models are illustrated in Fig. 20. A reasonably homogeneous medium is the result inferred from these data. The results presented in Fig. 20 were obtained via a constrained algebraic reconstruction technique (ART). Before this procedure was used, a generalized linear inverse algorithm was followed. However, for complicated models, this method yielded unphysical answers (negative $\sqrt{\epsilon_r}$) when applied to the real (noisy) data. The generalized linear inverse does indeed yield the best least-squares fit, but naturally occurring noise in the data can lead to "mathematically nice" but "physically unreal" results. By using a constrained algorithm,[9,10] the "degenerate but best" answers could be eliminated so that the "best physically real" answers could be determined. To further increase the resolution of the data-reduction procedure, we are also trying a simultaneous iterative reconstruction technique (SIRT).

2. The skin depth results indicate the uniformity of the coal, the coal/underburden interface, and the dipping coal bed.

The attenuation data are reduced by use of the formula

$$P_{rec} = \frac{P_{trans}\, G_{trans}\, A_{rec} \sin^4\theta}{4\pi R^2}\, e^{-2R/\delta},$$

which relates the power received (P_{rec}) to the power transmitted (P_{trans}). The quantity θ is the orientation angle between transmitter and receiver, R is the distance between transmitter and receiver, G_{trans} is the gain of the transmitter antenna, δ is the skin depth in the medium, and A_{rec} is the effective receiving area of the receiving antenna. Implicit in the use of this equation is the assumption that the medium is homogeneous and large enough in extent that there are no interfaces to scatter electromagnetic waves. If this is not the case, for small scale inhomogeneities one can approximate the transmitted wave in terms of differential segments. If the wave passes through a total distance R composed of N differential segments ($R_1, R_2, \cdots, R_N$), each with a slightly different skin depth ($\delta_1, \delta_2, \cdots, \delta_N$), then one can use the equation

$$P_{rec} = \frac{P_{trans}\, G_{trans}\, A_{rec} \sin^4\theta}{4\pi R^2} \exp\left[-\frac{2R_1}{\delta_1} - \frac{2R_2}{\delta_2} - \cdots - \frac{2R_N}{\delta_N} \right].$$

The same data-reduction algorithms used on the relative dielectric constant were used to determine δ_i. A sample of the preliminary results is given in Fig. 21. Again, the preshot data do not indicate much nonuniformity in the coal bed. The underburden

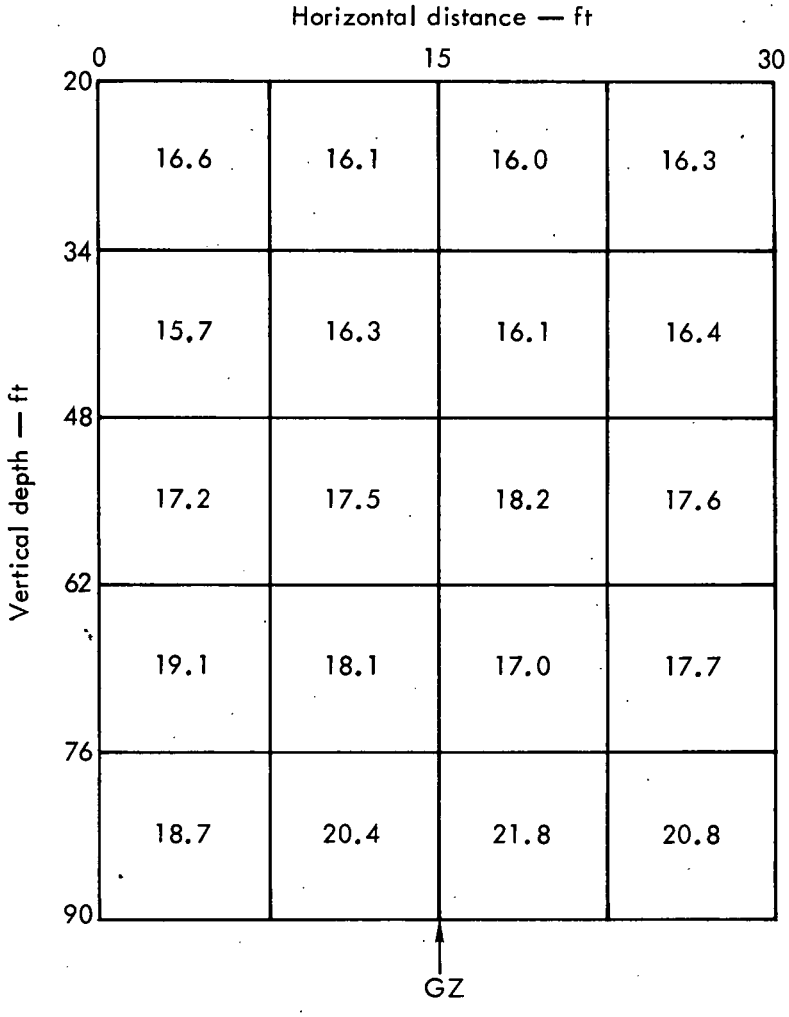

Fig. 20a. Complex models of ϵ_r (relative dielectric constant), assuming the layering pattern indicated in each case, can be inferred by using data-inversion algorithms on the Kemmerer transmission data for relative phase shift. The ϵ_r values are given in the boxes; 1 ft = 0.3048 m.

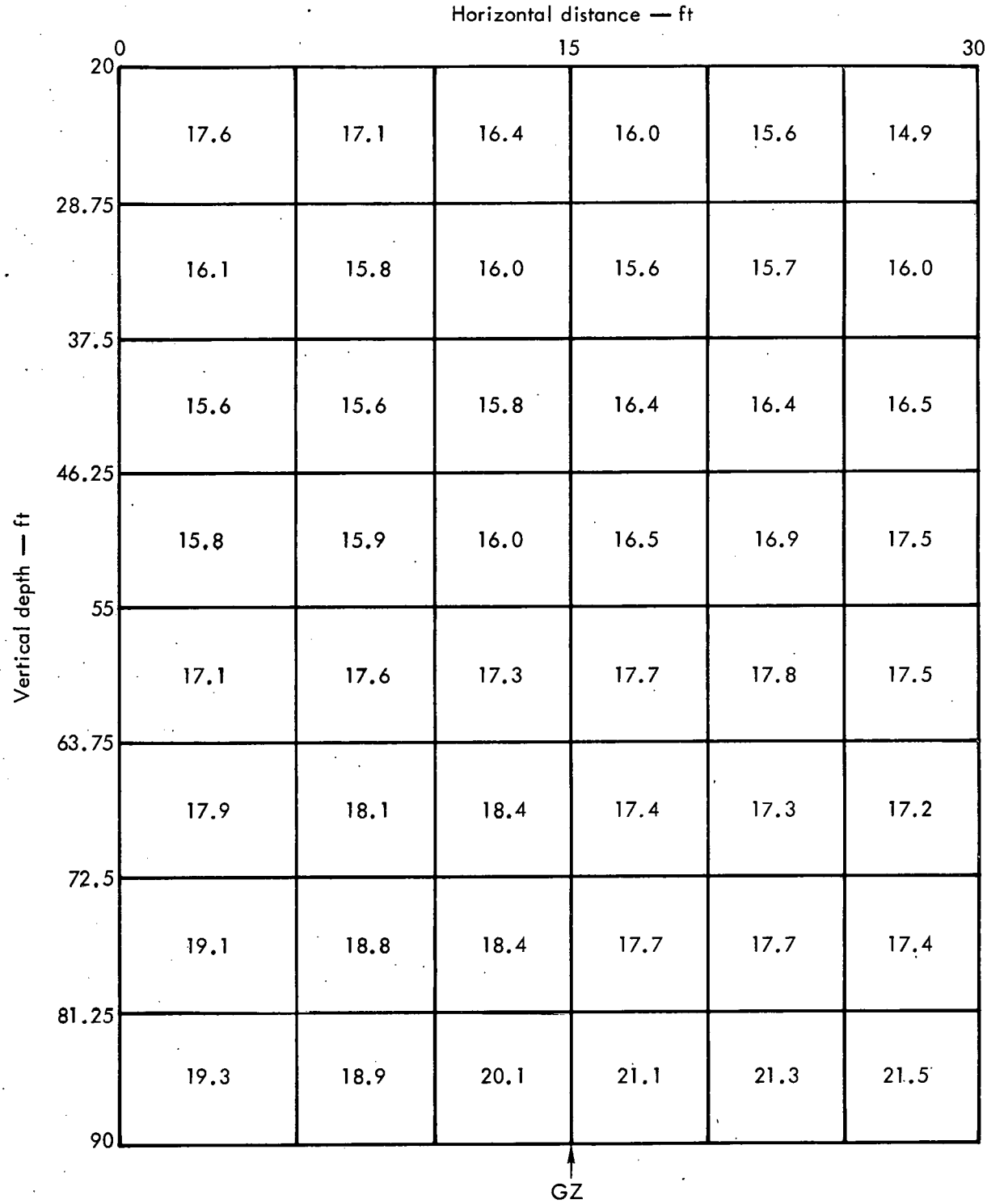
Horizontal distance — ft
0
15
30
20
28.75
37.5
46.25
55
63.75
72.5
81.25
90
Vertical depth — ft
17.6 17.1 16.4 16.0 15.6 14.9
16.1 15.8 16.0 15.6 15.7 16.0
15.6 15.6 15.8 16.4 16.4 16.5
15.8 15.9 16.0 16.5 16.9 17.5
17.1 17.6 17.3 17.7 17.8 17.5
17.9 18.1 18.4 17.4 17.3 17.2
19.1 18.8 18.4 17.7 17.7 17.4
19.3 18.9 20.1 21.1 21.3 21.5
GZ

Fig. 20b.

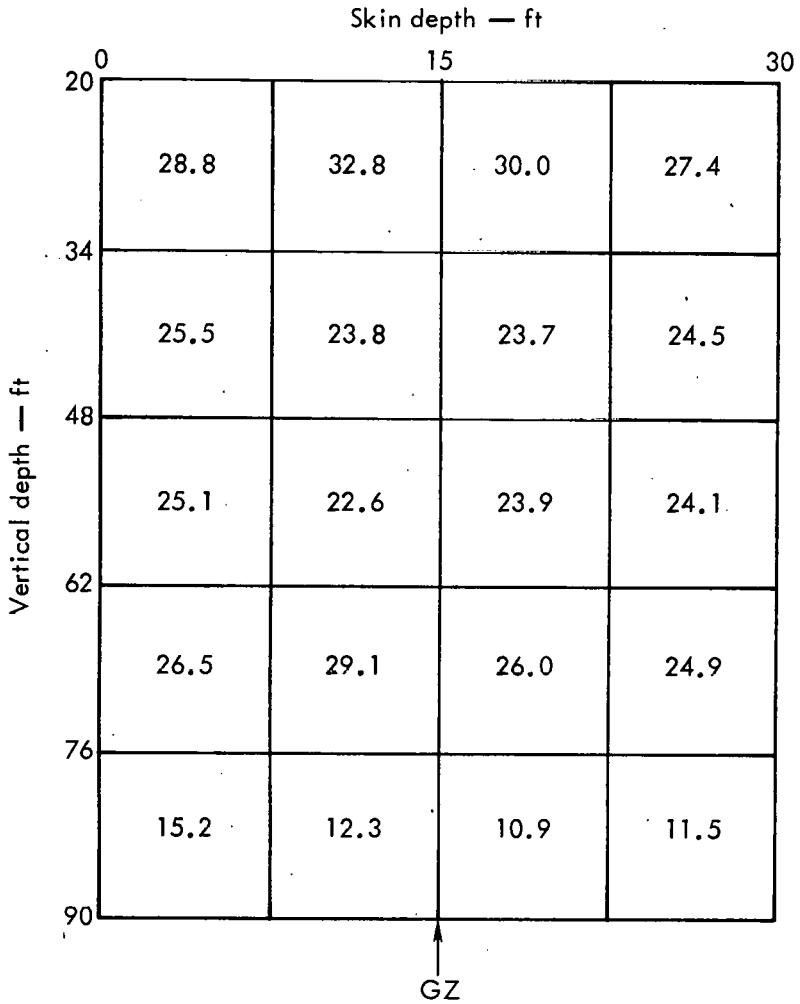

Fig. 21a. Complex models of δ (skin depth), assuming the layering pattern indicated in each case, can be inferred by using date-inversion algorithms on the Kemmerer transmission data for signal attenuation. The δ values are given in the boxes; 1 ft = 0.3048 m.

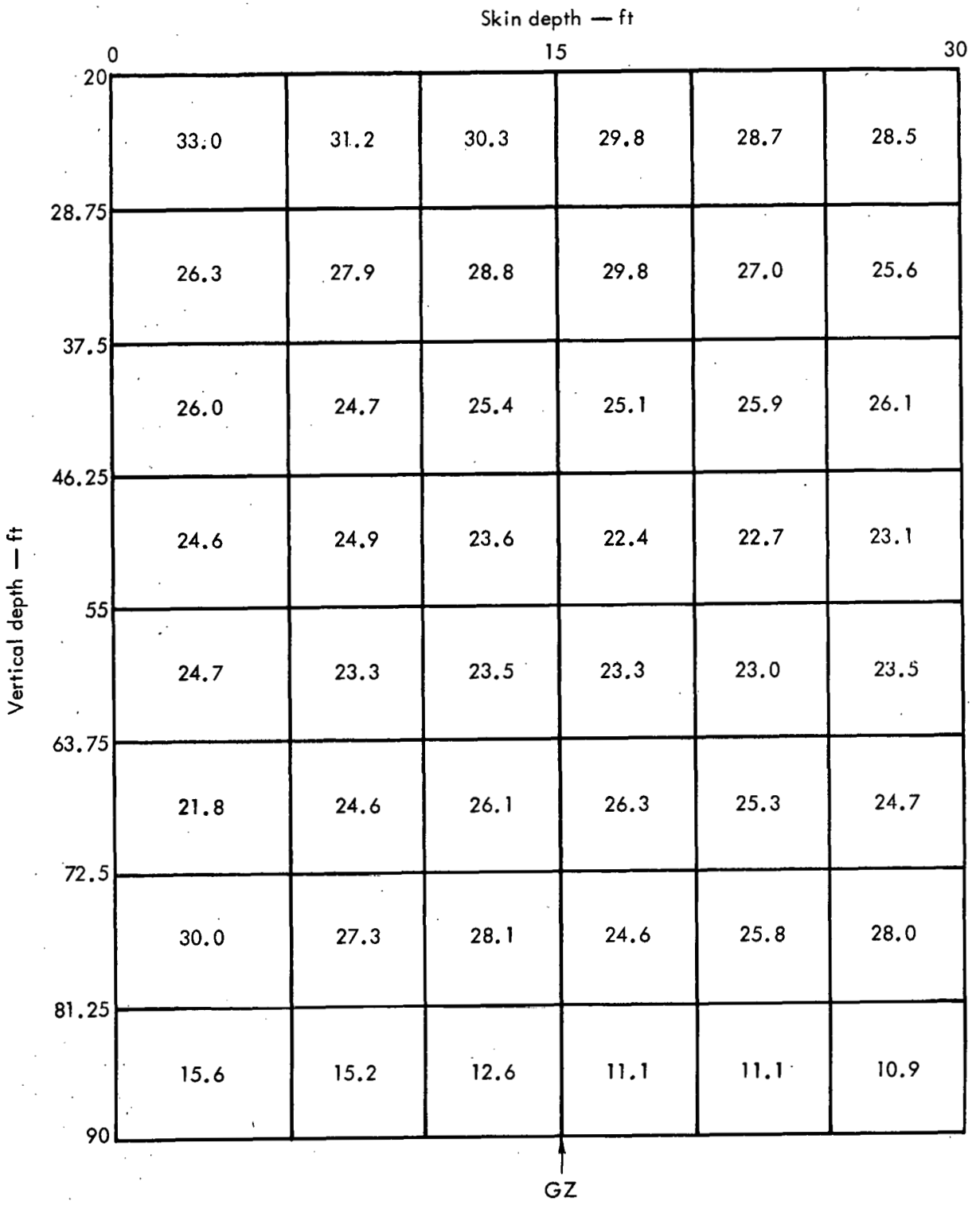
Skin depth — ft
0
15
30
Vertical depth — ft
20
28.75
37.5
46.25
55
63.75
72.5
81.25
90
33.0 31.2 30.3 29.8 28.7 28.5
26.3 27.9 28.8 29.8 27.0 25.6
26.0 24.7 25.4 25.1 25.9 26.1
24.6 24.9 23.6 22.4 22.7 23.1
24.7 23.3 23.5 23.3 23.0 23.5
21.8 24.6 26.1 26.3 25.3 24.7
30.0 27.3 28.1 24.6 25.8 28.0
15.6 15.2 12.6 11.1 11.1 10.9
GZ

Fig. 21b.

coal interface is clearly identified by the change of skin depth in the coal versus in the underburden. The dipping coal bed is indicated by the gradual change of skin depth, from left to right, in the lower layer of the more detailed model.

FUTURE WORK

1. Geophysical Modeling Facility

A well-conceived approach to solving problems in geophysics should be three-faceted. It should include in situ field experiments, laboratory scale-model experiments, and theoretical/numerical modeling. The procedures are supplementary in that insights may be easily discerned from one technique whereas another technique may be expensive, may require an inordinately large number of data points, or may require either a theoretical or experimental breakthrough. These techniques are also complementary in that a "new" method or results determined by one precedure can be substantiated by evidence obtained by an alternative procedure. LLL has much expertise in in situ field experiments and theoretical/numerical modeling but only limited experience in conducting scale-model electromagnetic geophysical experiments. However, electromagnetic methods of measuring geophysical phenomena can be easily scaled. Also, they have a wide range of applications (e.g., location of and definition of the extent of resources, monitoring time-changing subsurface conditions (e.g., burn front progression in coal gasification, earthquake prediction)).

For these reasons a facility is being constructed for scale-model electromagnetic measurements. With such a facility, not only the measurement schemes but also the subsurface conditions can be varied. This permits use of the facility for a wide variety of applications. In situ conditions (perhaps of complex structure) can be simulated and various experimental techniques can be tried to determine the "best" measurement precedure to attain the desired resolution. Controlled experiments can then be initiated to define the accuracy of the inversion algorithms (which reduce experimental data to a geophysical model).

Model experiments based upon electromagnetic methods can be conducted for a nominal investment. This is particularly true in that LLL has already instrumented a transient electromagnetic measurement facility.[11] This transient facility has a D112 minicomputer and associated peripheral equipment which permits analog-to-digital data conversion. This permits rapid and accurate acquisition and processing of experimental data. Plots of experimental results and processed data results can be routinely generated.

In addition, the available instrumentation enables the experimenter to conduct experiments in both the frequency and the time domains. Excitation frequencies from dc to 20 GHZ are readily available. Continuous-wave, swept-frequency, and pulse-excitation modes are readily performed with the present equipment. Controlled noise sources and correlators (both analog and digital) enable the experimenter to consider an even wider spectrum of measurement techniques.

Most of the instrumentation for this facility is already acquired. To complete the experimental setup, the following items are being purchased or built: water tank (~3 m (~10 ft square)) and 0.91 m (36 in.) deep)) with cover, fill hose, and drain pump; platform and steps surrounding the water tank; and miscellaneous equipment. Work has been started on the facility so that we can debug and calibrate the equipment and demonstrate the capability/versatility of the facility.

The measurement facility has immediate applications. For example, the subsurface structure at the Kemmerer, Wyoming site can easily be simulated. From the results we could easily determine the optimum probe spacings to discern subsurface anomalies induced by high explosives. One mode of the four-probe measurements at the site utilizes two drill holes. This experimental procedure is unique to LLL and is just starting to receive the attention of others. Thus, we need to develop rules of thumb for the best probe locations to resolve anomalies (particularly for unique subsurface features like those at Kemmerer). Some theoretical/numerical modeling can be performed for this procedure but the introduction of nonhorizontal bedding presents analytical nightmares.

A second application would be to put the theoretical/numerical modeling results generated by probabilistic potential theory[12] on firm footing (i.e., by demonstrating the degree of agreement between theory and experiment for known complex subsurface structure).

A third application would be to generate experimental data for a controlled situation. This data can then be used to test the reliability of inversion algorithms for a variety of controlled subsurface features. This is a simple way to demonstrate the total capability of the PPT/inversion algorithm; that is, the degree of resolution obtainable for specific subsurface conditions can be clearly demonstrated by the comparison of known subsurface conditions with the PPT/inversion algorithm results.

Other potential uses of the facility include: ground-circuit and ground-coupling problems of interest to DNA; demonstration of the feasibility of improved or new methods of locating and defining the extent of resources (e.g., ore bodies, geothermal areas), planetary exploration by surface probing, detection of anomalies (e.g., water pockets or the ore vein) from tunnels, communication from surface to subsurface (e.g., mine safety, submarine communication). The uses are unlimited. This effort is being developed under the auspices of the Electronics Engineering – Electronic Research Division.

2. Probabilistic Potential Theory

A novel analysis procedure – probabilistic potential theory (PPT)[12] – can be applied to electromagnetic problems in geophysics. It is based upon the duality between solutions to Laplace's equation (potential theory) and solutions to the random walk (or drunkard's walk) problem. PPT is particularly appropriate for geophysically inhomogeneous problems. The methods used to date suffer either from not being suitable for general inhomogeneities or from having excessive calculation requirements (e.g., time, storage, ease of progamming); PPT does not suffer from these limitations.

In fact, it is relatively easy to program on the computer, even for inhomogeneous regions; the duration of computing time can be adjusted to the accuracy required, and only the information needed to solve the problem is determined (i.e., no unneeded data are generated). This analysis method is being explored at LLL under the auspices of the Electronics Engineering—Electronics Research Division.

3. Additional Field Experiments

Whenever possible, field studies pertinent to the programs of interest should be undertaken. In this way, the validity of the various methods can be demonstrated and refined. As much lead-time as possible is desirable to permit intelligent experimental design and modification, and incorporation of improved methods into existing techniques. This requires field experiments at a number of sites under a variety of conditions. Murphy's Law really holds, especially in the field. Thus, the sooner you give Murphy a chance, the better your chances will be on the more difficult experiments.

A number of other ongoing LLL experiments would benefit by the techniques described here. The oil-shale and chalk-formation experiments are two that immediately come to mind. Given advance knowledge of such experiments, particularly statements of purpose, we could suggest known techniques or conceive technical concepts applicable to the problems at hand.

4. Data Interpretation Algorithms

Data interpretation is a very necessary art. It can best be performed by combining the experiences gained from previous field work, laboratory scale-model work, and theoretical/numerical analyses. From such combined experience, an intelligent experimental procedure specifically suited to the peculiarities of each site can be determined. This is the first step required to enable the experimenter to obtain data that decisively answer his questions.

Simulation models (first exact models and then noisy-data models) test the validity of the experimental procedure and thus should be tried before field experiments. The simulation models can be both experimental and theoretical/numerical; this can circumvent unwarranted (costly) in situ field experiments.

For the Kemmerer experimental methods used so far, we have tried theoretical/modeling using exact and noisy data to test the sensitivity of the various algorithms. The "bad" inversion schemes have been abandoned, and more promising inversion algorithms are presently being investigated. This process is never-ending, but it is proceeding toward what we regard as an "acceptable" inversion algorithm. Our successes and failures will be detailed in future reports.

CONCLUSIONS

1. Electrical methods can be used to advantage as a cost-effective procedure for initial site survey and selection.

2. Low-frequency methods should be used to ascertain the subsurface conditions. They are effective in many situations where higher-frequency methods are not. The LF methods can give good resolution.
3. High-frequency methods work in coal and can give good resolution. They are not inhibited by air spaces and may have much promise in monitoring the in situ burn front in coal gasification.
4. It may be possible to determine in situ permeability by electrically determining the velocity of propagation of a saline solution under pressure.
5. Sophisticated data inversion algorithms have been developed which give physically meaningful results when applied to real (noisy) data.
6. Laboratory scale-model experiments should be considered as an additional means of increasing insight in the relevant physical parameters (at much less cost than field studies).

ACKNOWLEDGMENTS

The authors are pleased to achnowledge the assistance and encouragement provided by a number of individuals. A major part of the mobilization required for collecting data as well as the actual process of data collection at Kemmerer was ably performed by Raymond W. Egbert. His enthusiasm for productive work is contagious. This work would not have been performed without the sponsorship of Douglas R. Stephens, who is responsible for LLL's in situ coal gasification program. Without the collective foresight and initiative of L. Lynn Cleland, Edmund K. Miller, John D. Salisbury, and Otto H. Krause, the work would not have come to fruition. It is a pleasure to acknowledge the on-site technical assistance of Joseph R. Hearst, Roger E. Lake, and Norman L. Hughes. The inversion of the HF data was assisted by the cogent and timely insights provided by John-Gilbert Huebel. The errors are those of the authors.

REFERENCES

1. R. J. Lytle, "Measurement of Earth Medium Electrical Characteristics: Techniques, Results, and Applications," IEEE Trans. Geosci. Electronics, GE-12, 81-101 (1974).
2. J. Lytle, E. Laine, D. Lager, and J. Okada, The Lisbourne Experiments: Propagation of HF Radio Waves Through Permafrost Rock, Lawrence Livermore Laboratory, Rept. UCRL-51474 (1973).
3. G. V. Keller and F. C. Frischknecht, Electrical Methods in Geophysical Prospecting (Pergamon Press, New York, 1966).
4. J. R. Inman, J. Ryu, and S. H. Ward, "Resistivity Inversion," Geophysics, 38, 1088-1108 (1973).
5. R. G. Van Nostrand and K. L. Cook, Eds. Interpretation of Resistivity Data, Geological Survey Profession Paper 499 (U.S. Government Printing Office, Washington, D. C. 20402, 1966). (A presentation of mathematical potential theory and practical field application for the direct current methods of electrical resistivity prospecting, 310 pages.)
6. J. L. Cramer, Lawrence Livermore Laboratory, private communication (1974).
7. A. G. Duba, Lawrence Livermore Laboratory, private communication (1974).
8. J. H. Pitts, Lawrence Livermore Laboratory, private communication (1974).
9. R. M. Mersereau and A. V. Oppenheim, "Digital Reconstruction of Multi-dimensional Signals From Their Projections," IEEE Proc. 62, 1319-1338 (1974).
10. IEEE Transaction on Nuclear Science NS-21 (June 1974). A special issue on physical and computational aspects of three-dimensional image reconstruction.
11. R. A. Anderson, J. A. Landt, F. J. Deadrick, E. K. Miller, The LLL Transient Electromagnetic Measurement Facility: A Brief Description, Lawrence Livermore Laboratory, Rept. UCID-16573, Rev. 1 (1974).
12. R. J. Lytle, R. M. Bevensee, and D. L. Lager, Three-dimensional Subsurface Delineation via a Novel Method for Determining the Subsurface Electrical Profile, Lawrence Livermore Laboratory, Rept. UCRL-51685 (1974).

APPENDIX: PRESHOT SUBSURFACE DATA FROM THE KEMMERER SITE

Subsurface LF Data

The LF (20 Hz) downhole data were taken with an equatorial dipole array and a monopole-dipole array (Fig. A-1). The data from the four holes surrounding the shot hole (see Fig. A-2) are given in Tables A-1 through A-3.

Subsurface HF Data

Photographs of the HF transmission loss and phase shift through the coal were taken for a number of transmitter-receiver locations in holes AR1-AR3 and AR2-AR4 (see Fig. 10 for an example of the photographs). These analog results were digitized for the 10-MHz and the 40-MHz readings of relative signal level and phase shift. The resulting digital data are given in Tables A-4 and A-5.

VE/cb/lmc

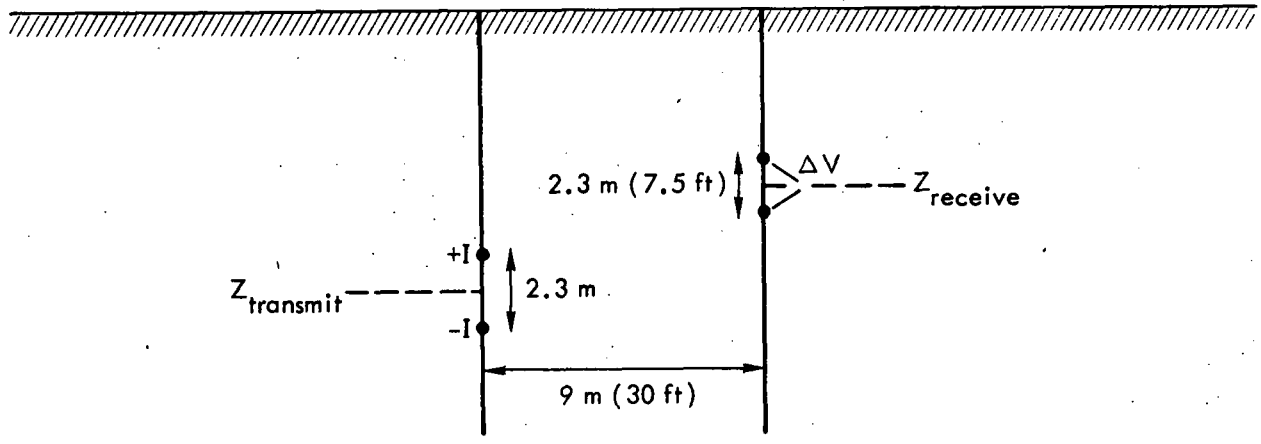

Equatorial dipole array

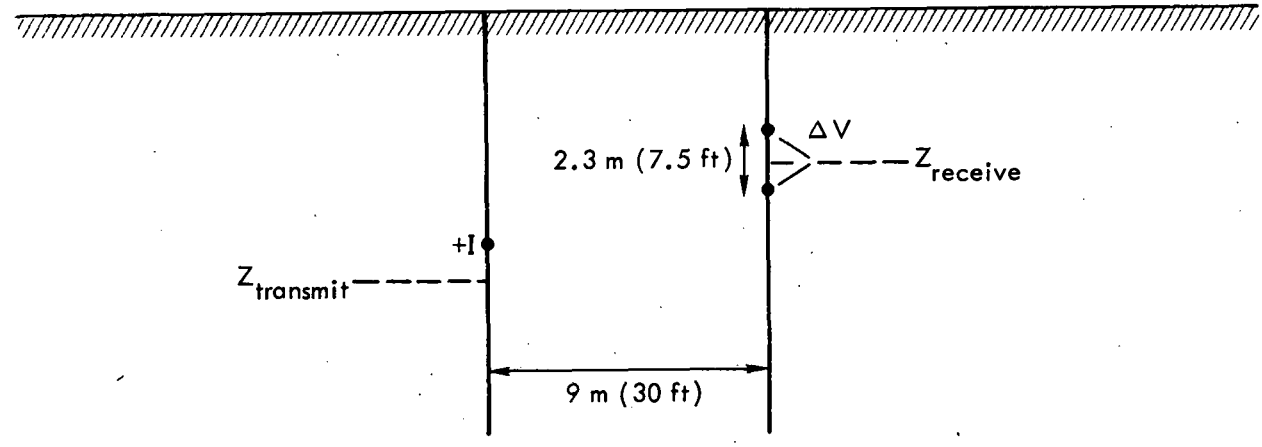

Monopole dipole array

Fig. A-1. Upper, physical configuration of the equatorial-dipole array. Lower, physical configuration of the monopole-dipole array.

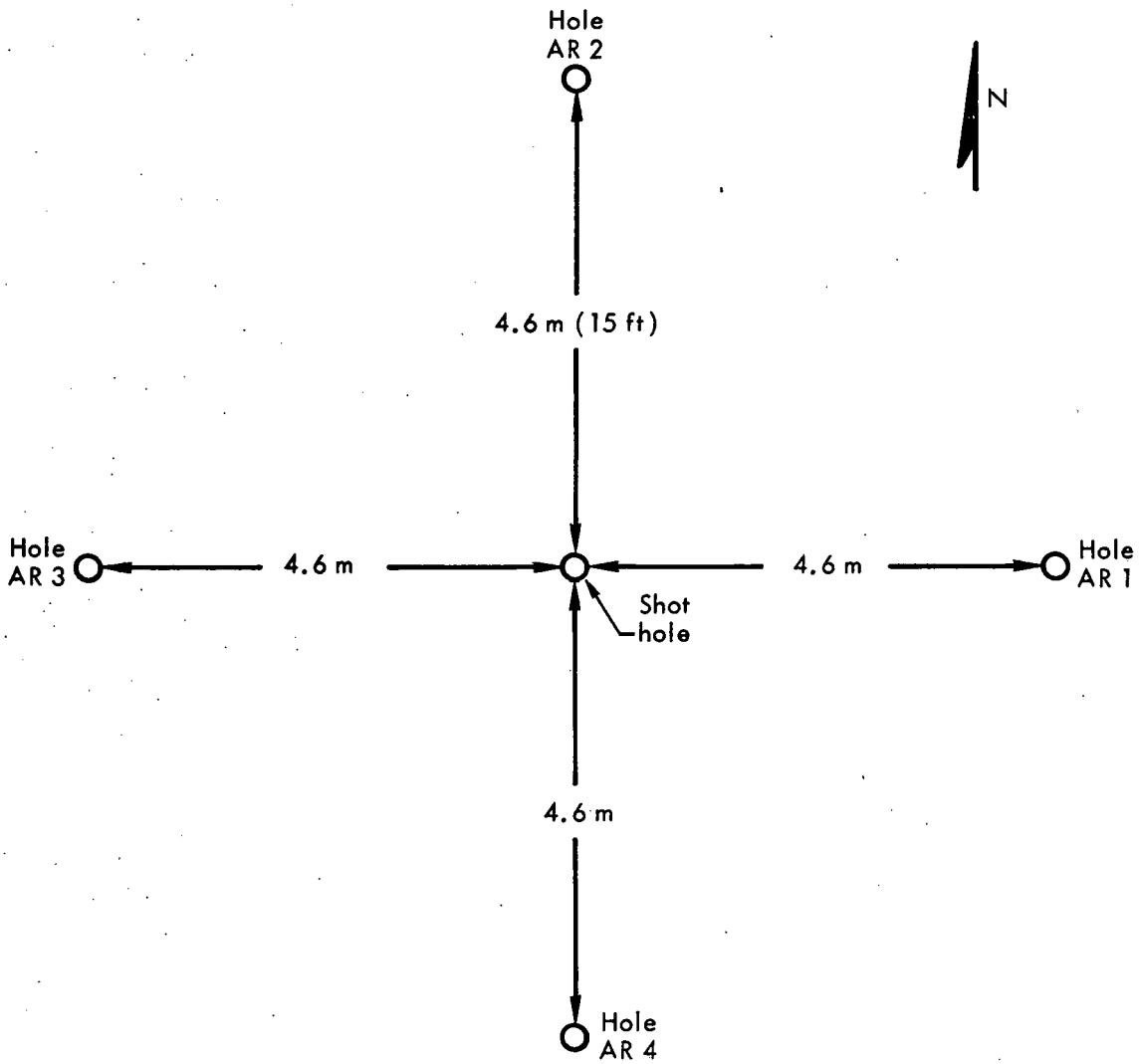

Fig. A-2. Location of experimental holes relative to the shot hole (GZ) for the arrays diagrammed in Fig. A-1.

Table A-1. The equatorial-dipole data for transmitter in hole AR3 and receiver in hole AR1. Data taken on October 5, 1974 at Kemmerer, Wyoming. The two drill holes were separated by 9 m (30 ft). The total length of each dipole array was 2.3 m (7.5 ft). (1 ft = 0.3048 m).

$Z_{transmit}$ (ft)	$Z_{receive}$ (ft)	$V_{receive}$ (mV)	$Z_{transmit}$ (ft)	$Z_{receive}$ (ft)	$V_{receive}$ (mV)
20.0	20.0	410.0	60.0	70.0	120.0
20.0	30.0	120.0	60.0	75.0	25.0
20.0	40.0	52.0	60.0	80.0	100.0
20.0	50.0	80.0	60.0	85.0	90.0
20.0	60.0	61.0	60.0	90.0	12.0
20.0	70.0	49.0	60.0	95.0	5.5
20.0	80.0	62.0			
20.0	90.0	4.5	70.0	20.0	48.0
20.0	95.0	1.6	70.0	30.0	67.0
			70.0	40.0	37.0
30.0	20.0	510.0	70.0	45.0	8.0
30.0	30.0	450.0	70.0	50.0	58.0
30.0	40.0	130.0	70.0	60.0	195.0
30.0	45.0	37.0	70.0	70.0	260.0
30.0	50.0	42.0	70.0	80.0	46.0
30.0	60.0	75.0	70.0	85.0	30.0
30.0	70.0	80.0	70.0	90.0	12.5
30.0	80.0	100.0	70.0	95.0	7.0
30.0	85.0	65.0			
30.0	90.0	7.5	80.0	20.0	41.0
30.0	95.0	2.4	80.0	30.0	65.0
			80.0	40.0	67.0
40.0	20.0	95.0	80.0	50.0	45.0
40.0	30.0	340.0	80.0	55.0	10.0
40.0	40.0	375.0	80.0	60.0	40.0
40.0	50.0	150.0	80.0	70.0	185.0
40.0	60.0	21.0	80.0	80.0	340.0
40.0	65.0	53.0	80.0	85.0	190.0
40.0	70.0	92.5	80.0	90.0	8.0
40.0	80.0	140.0	80.0	95.0	1.2
40.0	85.0	86.0			
40.0	90.0	9.0	90.0	20.0	24.0
40.0	95.0	5.2	90.0	30.0	42.0
			90.0	40.0	54.0
50.0	20.0	40.0	90.0	50.0	67.0
50.0	25.0	25.0	90.0	60.0	51.0
50.0	30.0	44.0	90.0	70.0	4.0
50.0	40.0	230.0	90.0	75.0	135.0
50.0	50.0	270.0	90.0	80.0	450.0
50.0	60.0	100.0	90.0	85.0	350.0
50.0	65.0	20.0	90.0	90.0	63.0
50.0	70.0	30.0	90.0	95.0	23.0
50.0	75.0	62.0			
50.0	80.0	110.0	95.0	20.0	19.5
50.0	85.0	65.0	95.0	30.0	34.0
50.0	90.0	9.5	95.0	40.0	44.0
50.0	95.0	3.5	95.0	50.0	57.0
			95.0	60.0	46.0
60.0	20.0	54.0	95.0	70.0	15.0
60.0	25.0	64.0	95.0	80.0	390.0
60.0	30.0	47.0	95.0	85.0	310.0
60.0	40.0	54.0	95.0	90.0	65.0
60.0	50.0	220.0	95.0	95.0	27.0
60.0	60.0	240.0			

Table A-2. The equatorial dipole data for transmitter in hole AR2 and receiver in hole AR4. Data taken on October 6, 1974 at Kemmerer, Wyoming. The two drill holes were separated by 9 m (30 ft). The total length of each dipole array was 2.3 m (7.5 ft) (1 ft = 0.3048 m).

$Z_{transmit}$ (ft)	$Z_{receive}$ (ft)	$V_{receive}$ (mV)	$Z_{transmit}$ (ft)	$Z_{receive}$ (ft)	$V_{receive}$ (mV)
20.0	20.0	450.0	50.0	80.0	88.0
20.0	30.0	250.0	50.0	90.0	69.0
20.0	35.0	75.0			
20.0	40.0	11.0	60.0	20.0	140.0
20.0	50.0	50.0	60.0	30.0	56.0
20.0	60.0	45.0	60.0	40.0	9.5
20.0	70.0	45.0	60.0	50.0	140.0
20.0	80.0	41.0	60.0	60.0	220.0
20.0	90.0	23.5	60.0	70.0	170.0
			60.0	80.0	7.0
30.0	20.0	310.0	60.0	90.0	60.0
30.0	30.0	490.0			
30.0	40.0	22.0	70.0	20.0	52.0
30.0	50.0	25.0	70.0	30.0	80.0
30.0	52.0	4.0	70.0	40.0	70.0
30.0	55.0	24.0	70.0	50.0	2.7
30.0	60.0	50.0	70.0	60.0	185.0
30.0	70.0	69.0	70.0	70.0	325.0
30.0	80.0	71.0	70.0	80.0	170.0
30.0	90.0	42.0	70.0	90.0	28.0
40.0	20.0	32.0	80.0	20.0	34.0
40.0	30.0	230.0	80.0	30.0	54.0
40.0	40.0	370.0	80.0	40.0	64.0
40.0	50.0	220.0	80.0	50.0	54.0
40.0	55.0	95.0	80.0	60.0	23.0
40.0	60.0	8.0	80.0	70.0	150.0
40.0	70.0	61.0	80.0	80.0	265.0
40.0	80.0	87.0	80.0	90.0	120.0
40.0	90.0	55.0			
			90.0	20.0	9.1
50.0	20.0	57.0	90.0	30.0	44.0
50.0	30.0	10.0	90.0	40.0	57.5
50.0	40.0	230.0	90.0	50.0	67.5
50.0	50.0	350.0	90.0	60.0	49.0
50.0	60.0	160.0	90.0	70.0	22.0
50.0	70.0	9.5	90.0	80.0	240.0
			90.0	90.0	320.0

Table A-3. The monopole-dipole data for transmitter in hole AR3 and receiver in hole AR1. Data taken on October 5, 1974 at Kemmerer, Wyoming. The two drill holes were separated by 9 m (30 ft). The total length of the dipole array was 7.5 feet. The transmitter (effectively a monopole) has a get-lost pin located approximately 600 ft. from ground zero, because this pin was in the overburden, the current introduced from it effectively was lost. (1 ft = 0.3048 m).

$Z_{transmit}$ (ft)	$Z_{receive}$ (ft)	$V_{receive}$ (mV)	$Z_{transmit}$ (ft)	$Z_{receive}$ (ft)	$V_{receive}$ (mV)
20.0	20.0	410.0	60.0	20.0	110.0
20.0	30.0	490.0	60.0	30.0	150.0
20.0	40.0	450.0	60.0	40.0	125.0
20.0	50.0	425.0	60.0	50.0	35.0
20.0	60.0	430.0	60.0	60.0	170.0
20.0	70.0	360.0	60.0	70.0	390.0
20.0	80.0	400.0	60.0	80.0	800.0
20.0	85.0	220.0	60.0	85.0	480.0
20.0	90.0	30.0	60.0	90.0	64.0
20.0	95.0	14.5	60.0	95.0	28.0
30.0	20.0	40.0	70.0	20.0	68.0
30.0	30.0	160.0	70.0	30.0	95.0
30.0	40.0	370.0	70.0	40.0	100.0
30.0	50.0	450.0	70.0	50.0	100.0
30.0	60.0	475.0	70.0	60.0	22.5
30.0	70.0	420.0	70.0	70.0	150.0
30.0	80.0	490.0	70.0	75.0	375.0
			70.0	80.0	750.0
30.0	85.0	270.0	70.0	85.0	470.0
30.0	90.0	35.0	70.0	90.0	73.0
30.0	95.0	16.0	70.0	95.0	31.0
40.0	20.0	180.0	80.0	20.0	34.0
40.0	30.0	125.0	80.0	30.0	50.0
40.0	35.0	12.0	80.0	40.0	60.0
40.0	40.0	120.0	80.0	50.0	82.0
40.0	50.0	350.0	80.0	60.0	78.0
40.0	60.0	480.0	80.0	70.0	24.0
40.0	70.0	490.0	80.0	75.0	160.0
40.0	80.0	620.0	80.0	80.0	500.0
40.0	85.0	320.0	80.0	85.0	390.0
40.0	90.0	45.0	80.0	90.0	72.0
40.0	95.0	19.0	80.0	95.0	35.0
50.0	20.0	145.0	90.0	20.0	12.5
50.0	30.0	175.0	90.0	30.0	18.0
50.0	40.0	70.0	90.0	40.0	21.0
50.0	50.0	140.0	90.0	50.0	32.0
50.0	60.0	360.0	90.0	60.0	35.0
50.0	70.0	490.0	90.0	70.0	28.0
50.0	80.0	700.0	90.0	80.0	100.0
50.0	85.0	390.0	90.0	85.0	95.0
50.0	90.0	52.0	90.0	90.0	24.0
50.0	95.0	23.0	90.0	95.0	19.0

Table A-4. HF data for transmission from holes AR1 ⇄ AR3 aligned along an east-west line and position 4.6 m (15 ft) (1 ft = 0.3048 m).

Transmitter depth (ft)	Receiver depth (ft)	10-MHz data		40-MHz data	
		Relative amplitude (dB)	Q^a	Relative amplitude (dB)	Q^a
90.0	60.0	-66.0	1.05	-76.0	1.2
90.0	70.0	-59.0	1.3	-63.0	1.35
90.0	80.0	-53.0	1.35	-57.0	1.5
90.0	90.0	-60.0	1.45	-78.0	1.6
90.0	100.0	-74.0	1.4		
80.0	50.0	-65.0	1.0		1.05
80.0	60.0	-56.0	1.3	-64.0	1.5
80.0	70.0	-51.0	1.5	-53.0	1.55
80.0	80.0	-47.0	1.6	-47.0	1.7
80.0	90.0	-57.0	1.35		
80.0	100.0	-71.0	1.2		
70.0	30.0	-71.0	0.95		
70.0	40.0	-66.0	1.1		1.15
70.0	50.0	-60.0	1.35	-62.0	1.45
70.0	60.0	-53.0	1.45	-53.0	1.5
70.0	70.0	-48.0	1.5	-48.0	1.65
70.0	80.0	-48.0	1.5	-50.0	1.65
70.0	90.0	-61.0	1.3		
70.0	100.0	-76.0	1.0		
60.0	30.0	-63.0	1.15		1.25
60.0	40.0	-59.0	1.4	-64.0	1.5
60.0	50.0	-53.0	1.4	-53.0	1.55
60.0	60.0	-49.0	1.45	-48.0	1.7
60.0	70.0	-49.0	1.65	-48.0	1.7
60.0	80.0	-53.0	1.3	-56.0	1.5
60.0	90.0	-65.0	1.1		
50.0	20.0	-63.0	1.2	-61.0	1.1
50.0	30.0	-56.0	1.4	-59.0	1.5
50.0	40.0	-51.0	1.55	-54.0	1.65
50.0	50.0	-49.0	1.7	-48.0	1.7
50.0	60.0	-50.0	1.65	-50.0	1.5
50.0	70.0	-56.0	1.3	-59.0	1.4
50.0	80.0	-61.0	1.1	-70.0	1.75
40.0	80.0	-68.0	1.0		
40.0	70.0	-60.0	1.1	-70.0	1.25
40.0	60.0	-56.0	1.3	-58.0	1.5
40.0	50.0	-50.0	1.6	-47.0	1.7
40.0	40.0	-49.0	1.7	-46.0	1.75
40.0	30.0	-49.0	1.6	-54.0	1.7
40.0	20.0	-55.0	1.5	-58.0	1.5
30.0	20.0	-50.0	1.55	-51.0	1.7
30.0	30.0	-48.0	1.7	-44.0	1.75
30.0	40.0	-48.0	1.6	-48.0	1.65
30.0	50.0	-54.0	1.3	-58.0	1.4
30.0	60.0	-62.0	1.1		1.2
30.0	70.0	-72.0	1.0		
20.0	20.0	-45.0	1.25	-45.0	1.75
20.0	30.0	-49.0	1.5	-46.0	1.5
20.0	40.0	-52.0	1.25	-58.0	1.4
20.0	50.0	-60.0	1.1	-73.0	1.15

[a] A phase shift of 360 deg requires a frequency sweep of $5 \times 10^6 \cdot Q$ Hz.

Table A-5. High frequency data for transmission from holes AR2 aligned along an north-south line and located 4.6 m 15 ft from either side of the shot hole.

Transmitter depth (ft)	Receiver depth (ft)	10-MHz data: Relative amplitude (dB)	10-MHz data: Q^a	40-MHz data: Relative amplitude (dB)	40-MHz data: Q^a
20.0	70.0	-72.0	1.0		
20.0	60.0	-63.0	0.95		
20.0	50.0	-52.0	1.1	-66.0	1.2
20.0	40.0	-44.0	1.3	-53.0	1.4
20.0	30.0	-41.0	1.55	-47.0	1.6
20.0	20.0	-36.0	1.6	-43.0	1.8
30.0	80.0	-72.0	0.75		
30.0	70.0	-64.0	1.0		
30.0	60.0	-54.0	1.0		1.15
30.0	50.0	-46.0	1.4	-54.0	1.35
30.0	40.0	-41.0	1.6	-45.0	1.6
30.0	30.0	-39.0	1.8	-40.0	1.65
30.0	20.0	-41.0	1.6	-47.0	1.65
40.0	90.0	-71.0	0.8		
40.0	80.0	-63.0	1.0		
40.0	70.0	-55.0	1.1	-68.0	1.1
40.0	60.0	-46.0	1.4	-48.0	1.35
40.0	50.0	-41.0	1.6	-49.0	1.65
40.0	40.0	-40.0	1.75	-42.0	1.7
40.0	30.0	-42.0	1.6	-48.0	1.6
40.0	20.0	-46.0	1.3	-58.0	1.4
50.0	90.0	-62.0	1.05		
50.0	80.0	-55.0	1.1		1.15
50.0	70.0	-53.0	1.4	-56.0	1.4
50.0	60.0	-42.0	1.55	-50.0	1.45
50.0	50.0	-41.0	1.75	-47.0	1.75
50.0	40.0	-44.0	1.55	-51.0	1.55
50.0	30.0	-48.0	1.4	-59.0	1.4
50.0	20.0	-55.0	1.15	-72.0	1.2
60.0	90.0	-54.0	1.1	68.0	1.2
60.0	80.0	-47.0	1.2	-57.0	1.3
60.0	70.0	-43.0	1.55	-47.0	1.5
60.0	60.0	-42.0	1.6	-47.0	1.6
60.0	50.0	-45.0	1.5	-52.0	1.5
60.0	40.0	-50.0	1.3	-64.0	1.4
60.0	30.0	-56.0	1.15		1.15
60.0	20.0	-63.0	1.0		
70.0	60.0	-53.0	1.5	-63.0	1.6
70.0	50.0	-52.0	1.35	-62.0	1.35
70.0	40.0	-59.0	1.15		
70.0	30.0	-66.0	1.0		
70.0	20.0	-72.0	0.9		
80.0	60.0	-59.0	1.3		
80.0	50.0	-58.0	1.1		
80.0	40.0	-66.0	1.0		
80.0	30.0	-74.0	0.8		
80.0	20.0	-74.0	0.7		
105.	105.	-66.0	1.00	-76.0	1.2

[a] A phase shift of 360 deg requires a frequency sweep of 5×10^6 Q Hz.